Aus der Klinik für Nuklearmedizin
der Medizinischen Fakultät Charité – Universitätsmedizin Berlin

DISSERTATION

Somatostatin receptor PET/CT in the management of patients with neuroendocrine tumors

zur Erlangung des akademischen Grades
Doctor medicinae (Dr. med.)

vorgelegt der Medizinischen Fakultät
Charité – Universitätsmedizin Berlin

von

Vikas Prasad

aus Patna, Bihar, Indien

Datum der Promotion: 14.10.2016 ....

1

Contents

Abstract

Somatostatin receptor PET/CT in the management of patients with neuroendocrine tumors

Differential somatostatin receptor (SSR) expression on neuroendocrine tumors (NET) makes it difficult to define an optimal place for SSR PET/CT in the management algorithm. With this background we aimed to a) validate SUVmax for the prediction of SSR density b) to correlate SSR PET/CT with non-invasive serum NETest to predict SUVmax on tumor lesions and c) to determine the utility of SSR PET/CT in the characterization and management of lung NET. **Methods**: For the validation of SUVmax for prediction of somatostatin receptor density, 31 surgical specimens of 25 NET patients were stained with SSR1, 2a, 4 and 5 antibodies. All patients underwent SSR PET/CT. For the correlation of NETest with SSR PET/CT, two independent datasets (27 and 22 patients, respectively), were evaluated. The role of SSR PET/CT for characterization and management of LNET was assessed in 27 patients (15 atypical carcinoids, 12 typical carcinoids). SUVmax of 186 lesions were measured and the detection rates of PET and CT were compared. **Results:** SUVmax was significantly correlated with immunohistochemistry for prediction of SSR2a density on tumor cells. NETest scores were predictive for PET-positivity with >95% concordance. Gene transcript expression was significantly correlated with SUVmax $(R^2=0.31$, RMSE=9.4). The gene MORF4L2 and SSR expression (SSR1, 3 and 5) exhibited the highest correlation with significant ROC-derived AUCs ($R^2=0.7$, $p<0.05$) for identifying progressive disease. 101/186 LNET lesions (54.3%) were depicted on both PET and CT, 53 lesions only on CT and 32 only on PET. SUVratio was significantly higher in AC as compared to TC (p<0.001). In patients referred for restaging, additional findings on PET lead to upstaging with change in management in 4/22 patients (AC, N=3; TC, N=1). In 4 patients (all AC) referred for restaging and in 1 patient (TC) referred for staging additional findings on CT missed on PET lead to correct staging. **Conclusions:** These results validate SUVmax as a reliable parameter for prediction of SSR density on NET lesions by PET imaging. NETest, significantly correlated with SSR PET-positivity, can be used as non-invasive test to predict SUVmax. Based on these correlations of SUVmax with SSR expression, SSR PET/CT revealed that typical and atypical LNET have different and complex patterns of metastases with variable SSR expression. Because SSR PET in addition to CT had significant impact on the treatment strategy in up to 18% of patients, it seems necessary to combine functional SSR PET and contrast-enhanced CT for appropriate restaging in LNET patients.

Abstract

Somatostatin-Rezeptor PET/CT im Patientenmanagement bei neuroendokrinen Tumoren

Eine differentielle Expression von Somatostatin-Rezeptoren (SSR) bei neuroendokrinen Tumoren (NET) erschwert es, eine SSR PET/CT optimal in den Patientenmanagementalgorithmus einzubauen. Vor diesem Hintergrund war unser Ziel a) SUVmax bezüglich seines Vorhersagewertes für die SSR-Dichte zu validieren, b) SSR PET/CT mit den Ergebnissen des nicht-invasiven Bluttests NETest zu korrelieren mit der Frage, ob dieser Test für eine Vorhersage des SUVmax von Tumorläsionen geeignet ist, und c) die klinische Wertigkeit der SSR PET/CT zur Charakterisierung und für das Patientenmanagement von Lungen-NET zu evaluieren. **Methodik:** Für die Validierung von SUVmax zur Vorhersage der SSR-Dichte wurden 31 Operationspräparate von 25 NET-Patienten mit Antikörpern gegen SSR1, 2a, 4 und 5 gefärbt und mit der SSR PET/CT verglichen. Für die Korrelation von NETest mit der SSR PET/CT wurden zwei unabhängige Datensätze (27 bzw. 22 Patienten) untersucht. Die Rolle der SSR PET/CT zur Tumorcharakterisierung und für das Patientenmanagement von Lungen-NET wurde an 27 Patienten (15 atypische Karzinoide (AC), 12 typische Karzinoide (TC)) untersucht. Dabei wurde der SUVmax in 186 Läsionen bestimmt und die Detektionsrate der SSR PET mit dem CT verglichen. **Ergebnisse:** SUVmax war zur Vorhersage der Rezeptordichte von SSR2a auf Tumorzellen signifikant mit der Immunhistochemie korreliert. NETest war prädiktiv für ein positives SSR PET/CT mit einer Konkordanz von mehr als 95%. Die Genexpressionsmuster waren dabei signifikant mit SUVmax korreliert (R^2=0,31, RMSE=9,4). Die beste Korrelation mit dem höchsten AUC in der ROC-Analyse (R^2=0,7, $p<0,05$) zur Vorhersage einer „progressive disease" erreichte das Gen MORF4L2 sowie die Expression von SSR1, 3 und 5. 101/186 LNET-Läsionen (54,3%) wurden sowohl im PET als auch im CT detektiert, weitere 53 Läsionen nur mit CT und 32 Läsionen nur mit PET. SUVratio war signifikant höher bei Patienten mit AC als bei TC ($p<0,001$). Im Rahmen des Restagings führten zusätzliche Befunde im PET zu einem Upstaging und einer Therapieänderung bei 4/22 Patienten (3 mit AC, 1 mit TC). Bei 4 AC-Patienten im Rahmen des Restagings sowie bei einem TC-Patienten im Rahmen des Stagings führten im CT erkannte Befunde, die sich nicht im PET nachweisen liessen, zu einem korrekten Staging. **Zusammenfassung:** Die Ergebnisse validieren SUVmax als einen zuverlässigen PET-Bildparameter zur Vorhersage der SSR-Rezeptordichte auf NET-Läsionen. NETest, signifikant korreliert mit einem positiven PET-Befund, kann als nicht-invasiver Test zur Vorhersage des SUVmax eingesetzt werden. Basierend auf diesen Korrelationen von SUVmax und SSR-Expression ließ sich mittels SSR PET/CT zeigen, daß typische und atypische LNET unterschiedliche und komplexe Muster in der SSR-Expression auf Metastasen aufweisen. Da die SSR PET in Ergänzung zur CT einen signifikanten Einfluß auf die Therapiestrategie in bis zu 18% der Patienten hatte, erscheint eine Kombination der funktionellen SSR PET mit einem Kontrastmittel-CT für ein optimales Restaging von Patienten mit LNET erforderlich.

1. Introduction

Neuroendocrine tumors (NET), a heterogeneous group of neoplasms, are characterized by their endocrine metabolism and specific histology patterns. Overexpression or high density of somatostatin receptors (SSR) on NET cells provides the rational for the development of synthetic somatostatin analogs for both diagnosis and therapy (1). SSR, however, are not uniformly expressed in a tissue specimen of NET (2) making immunohistochemistry in biopsy samples not a reliable method to predict the presence or absence of somatostatin receptors on tumors. In addition, the clonal differences of metastases in a patient necessitates whole body imaging with radiolabeled somatostatin analogs to assess the expression of SSR at different sites of metastases. During the last 10 years, major advancements in the development of high affinity radiolabeled peptides for PET imaging have been achieved, allowing detection of disease or tumor relapse at an early stage. However, the efficacy of therapeutic somatostatin analogs, like sandostatin and lanreotide, depends largely on the density of somatostatin receptors on tumor cells as shown by immunohistochemistry.

Despite its very high sensitivity (>90%) SSR PET/CT imaging is relatively costly and there is no common consensus as to how often SSR PET/CT should be performed in a patient with NET, who generally have a very good overall survival ranging between 5-10 years after initial diagnoses (1). To solve the dilemma, there is a scientific need to develop a reliable biomarker, which could predict the presence of NET at a very early stage and also predict the presence of SSR on tumor cells. NETest, an analog to liquid biopsy, is a novel test, which is highly successful in terms of both sensitivity and specificity in predicting the presence of NET as well as in defining the prognosis (3).

2. Aim of the study

With this background, this work constituted the following:

- Validation of maximum Standardized Uptake Value (SUVmax) on SSR PET/CT, using either ^{68}Ga-DOTATOC, ^{68}Ga-DOTATATE or ^{68}Ga-DOTANOC, as a reliable semiquantitative measure for the density of somatostatin receptors on tumor

specimens using manual and automated image analysis approaches in direct comparison to immunohistochemistry

- Correlation of SSR PET/CT imaging parameter SUVmax with the NET transcript signature
- Application of SSR PET/CT for characterization of lung NET tumors with respect to the underlying heterogenous SSR expression

3.   Materials and Methods

3.1   Validation of SUVmax for quantification of somatostatin receptor PET/CT

Validation of maximum Standardized Uptake Value (SUVmax) on SSR PET/CT, using either ^{68}Ga-DOTATOC, ^{68}Ga-DOTATATE or ^{68}Ga-DOTANOC, as a reliable semiquantitative measure for the density of somatostatin receptors on tumor specimens using manual and automated analysis approaches in direct comparison to immunohistochemistry (4).

3.1.1 Patients and Methods

Twenty-five NET patients who underwent elective surgery were retrospectively analysed in this study approved by the local ethics committee. All the patients were imaged with ^{68}Ga-DOTANOC (n=17) or ^{68}Ga-DOTATATE (n=8) PET/CT as part of the pre-operative staging procedure. All patients were examined using a dual modality PET/CT scanner (Biograph LSO Duo; Siemens). Patients were then operated and each single tumor lesion (N=31) was removed, marked and the histopathological results were correlated to the findings detected by ^{68}Ga-SSR PET/CT.

3.1.2 PET/CT

SSR PET/CT was performed in all patients according to the European Association of Nuclear Medicine guideline (5). The patients were scanned on a biograph duo (Siemens Medical Solutions, Knoxville Tenn,) approximately 60 minutes after i.v. injection of appximately 122 MBq (86-149 MBq) of ^{68}Ga DOTANOC or ^{68}Ga DOTATATE. Automatic region of interest for calculation of SUVmax and SUVmean on tumor was drawn on the tumor with the help of Siemens e.soft Nuclear Medicine Workstation.

3.1.3 Immunohistochemistry

Immunohistochemical analysis of tumor tissue was performed with specific polyclonal (for SSR1, 4 and 5 from Gramsch Laboratories, Schwabhausen, Germany) and monoclonal antibodies (for SSR2a from Epitomics, Burlingame, CA, USA). The detection of SSR-subtypes was performed using the labeled streptavidin-biotin-method (LSAB) and counterstaining was done with haematoxylin.

The analysis of the stained sections was performed using light microscopy according to the immunoreactive score (IRS) as described by Remmele and Stegner and to the Her2/neu DAKO scoring system.

In order to minimize the inter-observer bias, the immunohistochemical analyses was performed by two independent investigators on each tissue section. All the IHC slides were digitized using a VS120 slide scanner (Olympus® USA). Thereafter Definiens software (Definiens Developer XD and Definiens Tissue Studio®; Munich Germany) was used for the image analysis of the virtual tissue slides. Using the image analysis results, the calculation of user defined features in analogy to the Her2/neu score and to the IRS was performed.

Similar to the immunoreactive score of Remmele and Stegner, we developed a virtual score (Bad Berka Score 1; BB1), which is calculated by the percentage of cells with high marker intensity multiplied with the mean immunohistochemical marker intensity.

Overall, the immunohistochemical slides of 31 lesions from all 25 patients were digitized (31 each for SSR 1, 2a, 4 and 5). The SSR3 slides were not digitized due to logistical problems. From these 124 stained samples, 23 SSR1, 23 SSR2a, 25 SSR4 and 22 SSR5 slides were used as virtual slides for the present study.

3.1.4 Statistical Analysis

Statistical analysis was performed using Sigma Plot for Windows Version 11.0, Systat Software 2008. Spearmans' rank order correlation (r_s) was used to investigate correlations between automated and manually examined immunohistochemical image analysis results (IRS and Her2/neu scoring) and PET/CT uptake values. A p-value ≤ 0.05 was considered statistically significant.

3.2   NETest and SSR PET/CT

Correlation of SSR PET/CT imaging parameter SUVmax with the NET transcript signature (6)

3.2.1 Patient Characteristics

Two independent groups of metastatic NETs that demonstrated measurable disease on ^{68}Ga-SSR PET/CT were studied. Dataset 1 (n=27) included patients from Milan who were referred before peptide receptor radionuclide therapy (PPRT), which was performed as primary or salvage treatment (IEO Milan, IRST Meldola; Table 1). Dataset 2 (n=22) included patients who were referred to Charité - Universitätsmedizin Berlin for initial staging or restaging after various therapies. Table 1 shows the baseline demographic and disease characteristics of the whole group. All patients provided informed consent for the translational analysis which was authorised by the local Ethics Committee. Status at baseline was assessed according to RECIST 1.1 criteria.

3.2.2 SSR PET/CT

SSR PET/CT was performed following the European Association of Nuclear Medicine (EANM) Guidelines (5).

For set 1, a GE Discovery 600 (#1) Discovery ST (#2), Discovery LS (#3), or Discovery STE (#4) PET/CT scanner was used (GE Healthcare, Milwaukee, WI, USA) for imaging with [68]Ga- DOTATOC. The acquisition protocol included low-dose CT (120 kV, 80 mA, 0.8 s/rotation, 1.35 pitch, 3.75 mm slice thickness) for attenuation correction followed by the whole body PET scan (5-6 beds / 3 min each). Scanners #1,#2 and #4 acquired in 3-D mode (256x256 matrix, VUE point attenuation-weighted ordered subset expectation maximization (OSEM) algorithm, smoothing Gaussian filter), while scanner #3 acquired in 2-D mode (128x128 matrix, same reconstruction algorithm). For set 2 (17 patients with ^{68}Ga-DOTATATE, 4 patients with ^{68}Ga-DOTATOC) two different scanners were used. A Biograph 16 (Siemens AG, Erlangen, Germany; 120 kV, 230 mAs, 5-6 bed positions / 3 min, 0.75 mm collimation, and 0.75 slice thickness) was used from 2008-2009 (scanner A). Thereafter (2010 up to present) a Gemini TF-16 PET/CT (Philips Medical Systems, scanner B) was used. The 3-D line-of-response (LOR) algorithm of the system software was used to reconstruct the images (transaxial slices: 144x144 voxels, 4.0x4.0x4.0 mm3). A pre-scan low-dose CT was used for attenuation correction (120 kVp, 30 mAs).

Table 1: Baseline demographic and disease characteristics of the whole group

Patients	(n=48)
Age, median (range) in years	63,5 (32-77)
Men	26 (54%)
Time since diagnosis, in months (range)	0-212
Median	48
NET origin	
Pancreas	12 (25%)
Small bowel	22 (79%)
Colon	3 (6%)
Rectum	2 (4%)
Unknown	2 (4%)
MEN1	1 (2%)
Duodenum	1 (2%)
Tumor grade[†]	
G1 (Ki-67 0–2%)	14 (37%)
G2 (Ki-67 3–10%)	21 (55%)
Clinical stage	
IV	48 (100%)
Baseline RECIST status	
Progressive	29 (60%)
Stable	16 (33%)
n.a.	1 (2%)

Previous therapy	
Primary tumor surgery	33 (69%)
Somatostatin Analogs (SSA)	30 (60%)
Prior non-surgical treatment except SSA	16 (16)
PRRT	*12 (25%)*
Chemotherapy	*11 (23%)*
Liver directed therapies	*9 (19%)*
Targeted therapies	4 (8%)
Radiotherapy	*3 (6%)*
IFN	1 (2%)

3.2.3 Quantitative Image Analyses

PET images were interpreted by two nuclear medicine physicians, both with more than 10 years of experience each. The SSR expression in the tumor was assessed by calculating SUVmax using a spherical region of interest (ROI) in a transaxial attenuation corrected PET slice in those lesions that were positive on the visual assessment, i.e., uptake more than the immediate normal surrounding tissue. The uptake in normal liver tissue was used as a reference value for tumor SUVmax normalization. To avoid partial volume effects, only lesions larger than 1.5 cm in diameter, based on the co-registered CT were considered.

3.2.4 Multianalyte algorithm analysis (MAAA) PCR-based test (NETest)

Standardized MAAA PCR based test was performed as described in NETest. Four different learning algorithms trained on the internal training set using upregulated features were used and resulted in consensus categorization of samples into different groups using ''majority vote'' methodology. A NET score (0-8) was derived from the PCR data MATLAB (R2011a), Math Works, Natick, MA, USA); a value ≥ 2 is considered a positive tumor score (3).

3.2.5 CgA assay and Ki-67 proliferation index

CgA was measured using the DAKO CgA enzyme-linked immunosorbent assay (ELISA) kit (DAKO, Carpinteria, CA, USA). A cutoff of 19 units/l defined the upper limit of the normal range. The Ki-67 value was obtained from the original histopathological reports.

3.2.6 Statistical analysis

Comparative analysis of SUVmax, CgA, and Ki-67 across datasets 1 and 2 were undertaken using the Kolmogorov-Smirnov test of equality of continuous one dimensional distributions to determine if values of each parameter were drawn from the same underlying distribution, regardless of the data set origin. A two-sample test (null hypothesis: x and y drawn from the same continuous distribution) was performed; p values approaching 1 signified statistically identical distributions. Numerical predictions of Ki-67 and SUVmax using gene expression profiles were produced by fitting a generalized linear model via penalized maximum likelihood (''glmnet'') to the training data set (set 1), implemented in the ''caret'' R package (7,8). Model tuning parameters were estimated in caret by minimizing root mean square error (RMSE). Variable importance was calculated using the caret ''varImp'' function specific to the glmnet package. Regression models were tested on data set 2. In the instances where t variables (e.g., Ki-67 and CgA) were identified as noncompatible (significantly different) between data sets 1 and 2, the regression model was trained on the combined data set (data set 1 + data set 2) and model performances was estimated using five repeats of 10-tenfold cross-validation. Combinatorial assessments were undertaken using the SUVmax and MORF4L2 expression, Ki-67 and CgA. Sensitivity comparisons were undertaken using χ^2, nonparametric measurements and receiver-operating characteristic (ROC)/(AUC) (continuous variables) analysis. Both Prism 6.0 for windows (GraphPad Software, La Jolla, CA, USA, www.graphpad.com) and MedCalc Statisical Software version 12.7.7 (MedCalc Software, Ostend, Belgium, http://www.medcalc.org; 2013) were utilized. AUCS were compared and Z-statistic derived (MedCalc) (9).

3.3 SSR PET/CT in Lung NET(LNET)

Application of SSR PET/CT for characterization of lung NET tumors with respect to the underlying heterogenous SSR expression (10)

3.3.1 Patient selection

Between 1.1.2008 and 13.2.2014, 36 patients with LNET were referred for somatostatin receptor PET/CT; patients with aggressive LNET (SCLC, n=1; LCNEC, n=2) and those with unknown histopathology (n=6) were excluded. The remaining 27 patients with histologically proven atypical carcinoid (AC) n=15 and typical carcinoid (TC) n=12 were included in this retrospective analyses after approval by our local ethics committee. All patients were followed up for a minimum of 6 months after the date of PET/CT. Patients' characteristics are summarized in Table 2.

3.3.2 Somatostatin receptor PET/CT

For quantification of the somatostatin receptor expression in tumor and normal liver tissue maximum standardized uptake value (SUVmax) was used. SUVmax for both the tumor region and the normal liver was determined by using a manually drawn region of interest (ROI) in transaxial attenuation-corrected PET slices. The uptake in the liver was taken as reference value, and the SUVmax of the tumor lesions were normalised internally using SUVmax of the liver for normalisation according to the formula:

normalised Uptake in tumor (SUVratio) = SUVmax Tumor / SUVmax liver

SUV were measured only for those lesions that were definitely positive by visual assessment, i.e. the uptake of the lesion was higher than the uptake of the immediate normal surrounding tissue, and which had a size of more than 10 mm in diameter. For bone lesions, size was not taken into consideration according to RECIST criteria. The SUVmax values of SSR PET/CT can be influenced by several factors like difference in scanner type, acquisition and reconstruction parameters, and differences in the peptide affinity towards somatostatin receptors among others. For these reasons the normalised values (SUVratio) were preferred over SUVmax for describing the characteristics in the degree of somatostatin receptor expression in both metastases and the primary tumors.

3.3.3 Image Analyses

The PET/CT images were analysed in an interdisciplinary tumor board by experienced and board-certified physicians, primarily by a radiologist, and a nuclear medicine physician. For the image re-evaluation of this study, consensus of the two main readers,

nuclear medicine physician and radiologist, was considered sufficient. In case of discrepancy between these two readers, a second nuclear medicine physician was involved for a final decision. Data were put in clinical perspective with the pathologist, the attending gastroenterologist, and the surgeon. Lesions seen on PET/CT were characterised as tumor tissue or metastases only if all the physicians achieved a common consensus; in case of any discrepancy between the panellists, lesions were followed up with CT and/or MRI and by the clinical course. A tracer accumulation on PET images was defined as positive tracer uptake by visual assessment by the two observers. Lesions detected only by one modality (CT or PET) were termed positive or negative based on the follow-up or complementary imaging modalities like MRI and/or CT. Patients with mixed lesions had both receptor-positive lesions as well as receptor-negative lesions appreciable on CT only.

3.3.4 Statistical analysis

The R-software (version 3.1.3, R Foundation for Statistical Computing, Vienna, Austria) was used for statistical calculations. Categorical variables were analysed using contingency tables and chi-squared test. If the absolute frequency in contingency table cells was ≤ 5, Fisher's exact test was used. According to histograms and quantile-quantile-plots a non-parametric distribution of metric variables (SUVmax, SUVratio) was assumed and descriptive parameters are given as median, interquartile-range (IQR; 25th-quantil-75th-quantil) and range (minimum-maximum). Differences between un-paired groups were analysed using the non-parametric Kruskal-Wallis-test (> 2 groups) and the Mann-Whitney-U test (2 groups), respectively. The association of a metric and a dichotomous variable was analysed using receiver-operating characteristics (ROC) curves. The optimal cut-off value was defined by the point on the ROC curve with minimal distance to the point with 100% sensitivity and 100% specificity. All tests were performed as two-sided tests, and p-values of less than 0.05 were considered as significant.

4.   Results

4.1   Validation of SUVmax for quantification of somatostatin receptor PET/CT

4.1.1   Automated analysis of SSR

The BB1 score of SSR2a exhibited a significant correlation with the PET/CT parameters SUVmax (r_s: 0.41; p=0.049) and SUVmean (r_s: 0.50; p=0.019). With all other receptor subtypes the correlation factor was below 0.1 each indicating a not significant correlation.

4.1.2   Manually evaluated SSR data

The SSR2a expression as evaluated manually by means of the Her2/neu-score was significantly positively correlated to SUVmax (r_s: 0.42; P = 0.028) and SUVmean (r_s: 0.62; P < 0.001). In contrast, the SST2a expression as determined by the IRS score exhibited no significant correlation to SUVmax (r_s: 0.24; P = 0.224) and SUVmean (r_s: 0.34; P = 0.081). This was also the case for all other SSR subtypes (SSR1, 4, 5), which did not show any significant association to the PET/CT parameters.

4.2   NETest and SSR PET/CT

4.2.1   SUVmax vs IHC

Positive SSR PET/CT scans were available in all patients. Of 49 PET-positive patients, 47 (96%) exhibited a positive NETest, while only 26 (54%) had elevated CgA levels (χ^2=20.1, p< 2.5×10^{-6}). The MAAA score was significantly associated with image positivity (>95% concordance), while CgA levels were non-predictive.

4.2.2   Quality control and data processing: NETest vs SSR PET

We initially examined whether SUVmax, the circulating 51-gene expression profiles, plasma CgA levels, and tissue Ki-67 were statistically comparable between the two data sets. Principal component analysis of 51-marker gene expression profiles identified that one sample in the data set was an outlier. This sample, a bronchial tumor of small cell lung cancer (SCLC), was removed. Results of the two-sample Kolmogorov-Smirnov test of equality indicated that SUVmax values were comparable (p=0.546) between the two

data sets, while neither CgA (p=0.165) nor Ki-67 values (p=0.0535) were mathematically comparable (Figure-1). Based on the mathematically defined acceptable comparability of SUVmax, we then merged the two data sets to mathematically amplify data analysis.
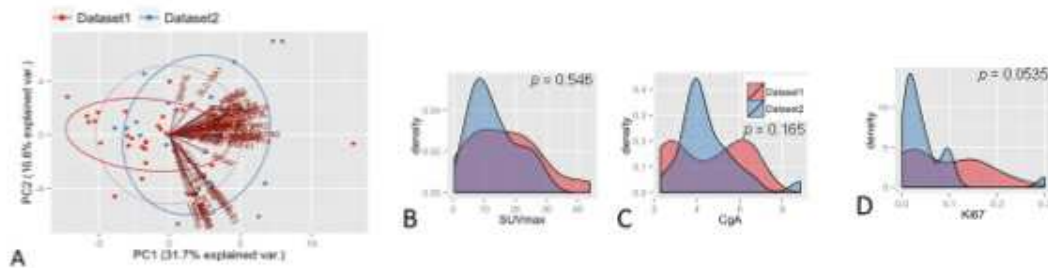

Figure 1: Principal Component Analysis of dataset-1 and dataset-2 (**1A**) using expression profiles of 51 marker genes. One outlier sample was excluded. Distribution densities of SUV (**1B**), CgA (**1C) and** Ki-67 (**1D**) in datasets-1 and 2 confirmed the comparability of SUV$_{max}$, but not of Ki67 or CgA.

4.2.3   CgA and Ki-67

Although CgA levels were poorly reproducible (Kolmogorov-Smirnov p=0.165) between the two data sets, utilizing the mathematical model of 'feature importance selection,' SLC18A2 and LED1 were identified as circulating marker transcripts that could be used to predict CgA levels (R^2=0.13 and RMSE=1.47; Figure 2). No relationship could be identified between Ki-67 and CgA or between SUVmax and Ki-67 using the same modeling approaches.
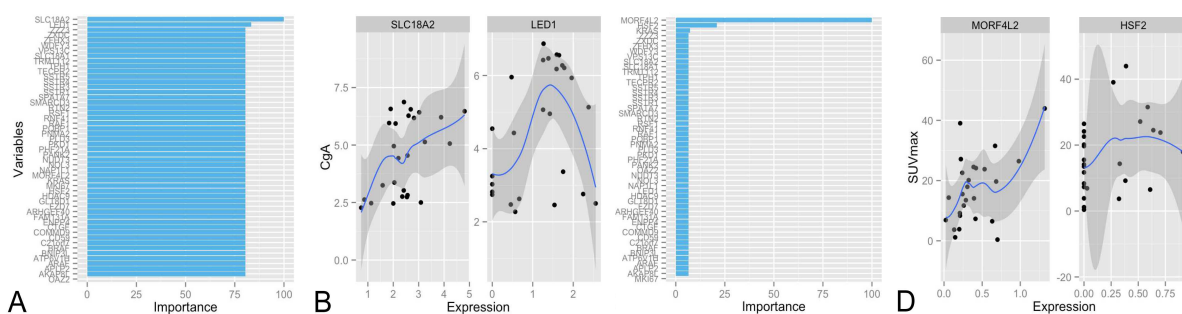

Figure 2: Bar plots of top-contributing genes to prediction of CgA and SUVmax levels (**2A, C**). Scatter plots of expression levels of top contributing genes and CgA and SUVmax levels in dataset-1 (**2B, D**). SLC18A2 and LED1 were identified as key marker genes for CgA, while MORF4L2 was the most effective predictor of SUV$_{max}$. Linear regression lines for each scatter plot are shown in blue, while the 95% confidence regions are shaded in grey.

4.2.4 Somatostatin receptor imaging

We next examined whether circulating marker gene expression could be used to predict SUVmax. Given that SUVmax values were comparable between the two data sets, data set 1 was used to train the generalized linear regression model, while data set 2 was used as a test. In the training model, the transcript MORF4L2 was the most effective predictor of SUVmax. A regression of $R^2=0.31$ and RMSE=9.4 was identified. An assessment of the combined data set indicated that among expression levels, SSR1, 3 and 5 were the single most important predictor of SUVmax ($R^2=0.15$ and RMSE=9.5). Neither CgA levels nor Ki-67 were predictive of SUVmax. To examine whether circulating marker levels and imaging could be used in combination, we evaluated different combinations of gene expression levels and SUVmax to predict disease status, e.g. stable disease according to RECIST1.1 criteria. Only the MORF4L2-calculated quotient (a combination of circulating transcript expression and SUVmax) was significantly elevated in progressive disease (p<0.03) (Figure 3).
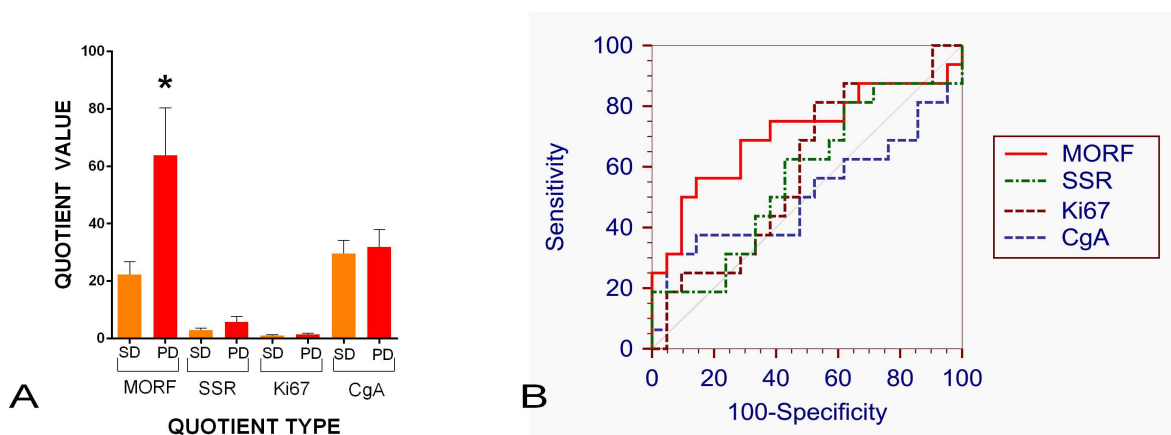

Figure 3: Expression differences and receiver operating characteristic (ROC) curves for the four different quotients. **3A**) The MORF4L2-quotient value was significantly increased in patients with progressive disease (PD; n=24) compared to those with stable disease (SD; n=25). **3B**) The AUC for the SUVmax: MORF4L2 quotient was 0.71 compared to quotients assessing averaged SSR expression and either the Ki-67 index or CgA. *p<0.05 vs. stable disease. MORF = MORF4L2 quotient, SSR = averaged SSR expression quotient, Ki67 = Ki-67 indexed quotient, CgA = chromogranin A-calculated quotient.

4.3 SSR PET/CT in Lung NET

4.3.1 Histopathology

Patient's histopathology was classified according to the grading system proposed by Rindi et al (11). Based on this classification, 12 patients had TC (44.4%) and 15 had AC (55.6%).

Assessment of Ki-67 in tumor tissue (13 primary tumor; PT, 17 metastases) was available in 23 patients (8 TC, 15 AC). In 6 patients Ki-67 was available from different sites at different time points. The median proliferation rate (Ki-67) in metastases (10.0; IQR, 5.0-15.0; n=17) was significantly higher compared to primary tumors (5.0; IQR, 2.0-10.0; n=13) (p=0.035) (see Figure 1). The median time interval of 31.9 months (IQR, 17.2-44.1) between SSR PET and Ki-67 evaluation in specimens was relatively long, which could have been partially responsible for the aforementioned significant difference in the Ki-67 of metastases and primary tumor.

4.3.2 PET vs. CT - Lesion Based Analysis:

Because of the retrospective nature of the study and ethical issues, none of the discordant lesions had histopathological confirmation. The discrepant lesions between PET and CT were confirmed by clinical follow-up for at least 6 months and, wherever needed, also with further correlative imaging (CT, MRI or PET).

Overall, 186 lesions were analysed: 29 lesions in lungs suspected to be primary tumors (N=6 patients, 3 with multiple lung nodules sub-classified as diffuse pulmonary neuroendocrine cell hyperplasia (DIPNECH), bone 52, LN 29, liver 49, other metastases 27. 101 lesions (54.3%) were concordant (both PET and CT demonstrated the lesions) whereas 53 (28.5%) lesions were only visible on CT and 32 (17.2%) lesions were only positive by PET (Table 2). Lesions only positive in PET were significantly more frequent in AC patients (30/148=20.3%) compared to TC patients (2/38=5.3%; p=0.028).

PET failed to detect 21/29 lung lesions. PET detected 9/49 (18.4%) additional liver metastases, which were not visible on CT. In contrast, CT picked up 23/49 additional

liver lesions (46.9%) not seen on PET (somatostatin receptor negative). One lesion seen on CT was later classified as a liver cyst on biopsy. In this patient, all the lesions seen on CT had the same characteristics as the lesion biopsied and therefore, all these lesions were considered as cysts. Two additional lymph node metastases (6.9%) were seen on PET while CT picked up 9/29 (31%) pathologically enlarged lymph nodes confirmed as metastases on follow-up. CT missed 17/52 bone lesions (32.7%) whereas PET depicted all 52 bone lesions (results are summarised in Table 2).

Table 2: Absolute and relative frequency of concordant and discordant lesions on PET/CT. *3 DIPNECH patients with multiple lung nodules are also included.

	Only positive on PET	Only positive on CT	Concordant positive on PET and CT	Total
Primary Tumor*	0 (0%)	21(72.4%)	8 (27.6%)	29 (15.6%)
Liver	9 (18.4%)	23 (46.9%)	17 (34.7%)	49 (26.3%)
Bone	17 (32.7%)	0 (0%)	35 (67.3%)	52 (28.0%)
Lymph Node	2 (6.9%)	9 (31.0%)	18 (62.1%)	29 (15.6%)
Others	4 (14.8%)	0 (0%)	23 (85.2%)	27 (14.5%)
Total	32 (17.2%)	53 (28.5%)	101 (54.3%)	186 (100%)

SUVmax of SR positive tumor lesions (133/186) were normalized to the SUVmax of the liver to generate normalized SUV (SUVratio) values. SUVratio was significantly higher in AC (median/ IQR/ range, 1.7/ 0.7-2.4/ 0.2-6.4) as compared to TC (median/ IQR/ range, 0.5/ 0.3-0.6/ 0.2-2.6; p<0.001) with respect to all lesions (N=133; PT 8; Metastases 125;. AC metastatic lesions (median/ IQR/ range, 1.7/ 0.8-2.4/ 0.2-6.4) also showed significantly higher SUVratios as compared to TC (median/ IQR/ range, 0.4/0.3-0.6/ 0.2-2.0; p<0.001).

4.3.3. PET vs. CT - Patient Based Analyses. Frequency and characteristics of metastases:

The frequency of metastases in patients with AC (13/15; 86.7%) was higher compared to patients with TC with a trend towards significance (6/12; 50%; p=0.087). In patients with AC, 4/15 had mixed lesions, 3/15 had somatostatin receptor negative lesions, 2/15 had no detectable lesions on SSR PET whereas in the remaining 6/15 patients all the lesions were somatostatin receptor positive. In patients with TC 1/12 had mixed lesions, 1/12 had PET-negative lesions, 7/12 had no detectable lesions on SSR PET whereas in

the remaining three patients all the lesions were somatostatin receptor positive (Table 3). Frequency of patients with mixed lesions was not statistically significant between TC (1/12=8.3%) and AC (4/15=26.7%; p=0.34). This was also true analysing only patients with metastases (TC vs. AC, 1/6=16.7% vs 4/13=30.8%; p=1).

Table 3: Absolute and relative frequencies of somatostatin receptor-positive and somatostatin receptor-negative lesions in AC and TC patients

Histopathology	All negative	All positive	Mixed Lesions	No Metastases	Total
TC	1 (8.3%)	3 (25%)	1 (8.3%)	7 (58.3%)	12
AC	3 (20.0%)	6 (40.0%)	4 (26.7%)	2 (13.3%)	15
Total	4 (14.8%)	9 (33.3%)	5 (18.5%)	9 (39.3%)	27

Bone metastases were present only in AC (N=6) but not in TC patients, and all bone metastases were SSR PET-positive lesions.

4.3.4 Effect of PET on management strategy

Additional findings on PET missed on CT lead to upstaging in 4 patients (AC N=3; TC N=1; all restaging) resulting in a change of the management strategy (Table 4). Two patients (1 AC, 1 TC; Table 5) with liver metastases but no extrahepatic lesions were treated with transarterial embolization and afterloading of the liver, in one patient (AC) salvage PRRT was ruled out because of stable disease in bone, and in the 4th patient (AC) a wait-and-watch policy was applied because of low tumor burden.

In 4 patients referred for restaging (all AC) and in 1 patient referred for staging (TC) additional findings on CT missed on PET lead to correct staging (Table 4). In patients referred for restaging, additional findings on PET lead to upstaging with change in management strategy in 4/22 (18.2%) patients. In one patient (Table 4, pat. #8), one of the liver lesions seen on CT was biopsied and was confirmed to be free of malignancy. All the lesions in this patient were found to be somatostatin receptor negative and the disease was downstaged correctly by PET.

4.3.5 Patients with multiple lung nodules:

Three of 27 patients (11.1%) had multiple lung nodules and were subclassified into DIPNECH by the tumor board based on initial findings and the follow-up results. All the lung nodules diagnosed on CT were subclassified as primary tumors due to the absence of histopathological confirmation. One patient presented with 9 lymph node metastases being all positive on both PET and CT. However, only 6/26 (23.1%) lung lesions ranging in size from 6-26 mm were found to be somatostatin receptor positive with very low SUVmax (Table 6) in these patients with DIPNECH.

Table 4: PET and CT results (SD: Stable Disease, LN: lymph nodes, PT: primary tumor, TAE: transarterial embolisation, PRRT: peptide receptor radionuclide therapy, SR: somatostatin receptor, TC: typical carcinoid, AC: atypical carcinoid, M: male, F: female, NA: not available; * staging; ** restaging)

Patient-ID	Sex	Age	Histo	Ki67	Additional CT Information	Additional PET information	Change in Management due to PET
PET leading to correct staging							
#27**	M	67	AC	2	-	1 Liver, 2 Bone	SD Bone, no salvage PRRT indicated
#8**	F	63	AC	3		Liver Cysts	Follow-up, without intervention
#28**	F	34	AC	15	-	3 Bone 3 Others,	Low tumor burden, wait and watch, no PRRT
#29**	F	68	TC	5	-	2 Liver	Afterloading of liver metastases
#31**	F	53	AC	20	-	2 Bone	TAE of liver metastases seen on CT and SR PET because of low tumor burden on bone
CT leading to correct staging							
#1**	F	74	AC	10	1 recurrent tumor in lung 9 LN	-	-
#10*	F	58	TC	NA	8 PT	-	-
#12**	M	59	AC	10	5 Liver	1 LN	-
#30**	F	50	AC	10	7 Liver	-	-

Table 5: Patients' characteristics with confirmed liver metastases on CT or PET in follow-up

	Pat. 4	Pat. 12	Pat. 20	Pat 27	Pat 29	Pat. 30	Pat. 31	Pat 35
Ki67, histo	15%, AC	10%, AC	5%, AC	10%, AC	1%, TC	10%, AC	20%, AC	7%, AC
Lesion Size (mm)	7-32	14-40	20-150	-	-	15-62	21-23	15-19
SR +ve lung lesions	19/24	0/5	5/5	1/1	2/2	0/7	2/2	2/2
CT +ve lesions	21/24	5/5	4/5	0/1	0/2	7/7	2/2	2/2
SUVmax	7.4-17.4		-	5.2-10.5			16.2-44.4	16.5-17.5

Table 6: Characteristics of patients with diffuse pulmonary neuroendocrine cell hyperplasia (DIPNECH). Lesion size and SUVmax are described by minimum-maximum values

	Patient 3	Patient 10	Patient 25
Ki67	5%	NA	15%
Transformation	TC	TC	AC
Lesion Size (mm)	2-18	2-26	2-26
SR +ve lung lesions	4/13	0/8	2/5
SUVmax	1.4-7.9	-	1.0-2.5
LN-Metastases on SR-PET and CT	-	-	9/9

5. Discussion

In the absence of evidence-based consensus guidelines on the management of LNET, the current standard of practice varies appreciably according to the availability of diagnostic tools: contrast-enhanced CT is standard in virtually all LNET patients often followed by somatostatin receptor scintigraphy or SSR PET/CT. The role of SSR scintigraphy in comparison to CT has been prospectively evaluated in only one study consisting of 16 patients with LNET (15 TC and 1 AC) after bronchial carcinoid resection (12). SSR scintigraphy was found to be useful in 2/16 patients (12.5%) whereas CT was found to be of additional benefit to SSR scintigraphy in 1/16 patient. The lack of standardised imaging tools in the management of LNET is partly attributable to their rarity as well as to their heterogeneous nature.

An important attribute of tumor heterogeneity of LNET is the differential somatostatin receptor expression, partially depending on tumor grade. An important scientific question often raised during clinical discussion is whether the radiopharmaceutical uptake measured on PET/CT by means of SUV correctly represents the somatostatin receptor density on the tumor, a prerequisite for therapy with cold or radiolabeled somatostatin agonists. We could show, based on both manual as well as state of the art digital pathology, that the SUV of a tumor lesion correctly measures the somatostatin receptor density even at the microscopic level. This is in line with previous studies which have also shown that SUV, especially SUVmax, is a reliable parameter for the in-vivo assessment of SSR expression on tumors based on immunohistochemistry and also correlates with quantitative polymerase chain reaction for gene expression of SSR2 (13), and that heterogeneous uptake of ^{68}Ga-DOTATOC or ^{68}Ga-DOTATATE could be a reliable parameter to predict response to treatment and prognosis. Our study for the first time showed that digital pathology can be used reliably for quantification of SSR2a as well.

Based on these clinically relevant findings we applied SSR PET/CT for characterization of primary LNET and their metastases by imaging. AC patients with intermediate grade tumors, although not significant, were found to have a higher proportion of mixed lesions, i.e. both somatostatin receptor-positive and -negative lesions as compared to

TC patients, which had a more homogeneous somatostatin receptor expression. Interestingly, our findings regarding the degree of somatostatin receptor expression on TC and AC tumor lesions are contradictory to previous studies (14,15,16). In our analysis, TC lesions had a significantly lower SUVmax and SUVratio than AC lesions whereas the previously published studies reported significantly higher SUVmax in TC as compared to AC (14,15,16). This difference could be primarily due to the difference in the patient populations. While in our analysis, most of the patients (22/27; 81.5%) underwent SSR PET/CT for restaging after primary tumor resection, in the study from Kayani et al. (14) 83% (15/18) of the patients underwent SSR PET/CT for initial staging, and the study of Venkitaraman et al. (15) considered only patients (N=26) referred for staging. Furthermore, the ratio of TC (44%) vs. AC (56%) in our population is quite different in comparison to Kayani's group (14) with 72% TC (N=11) vs. 11% AC (N=2) or Venkitaraman et al. (15) (TC=81%, N=21 vs. AC 19%, N=5). In their analysis of SUV in TC and higher grade LNET, Kayani et al. (14) categorized SCLC and NSCLC with NET differentiation into one group and LCNEC together with AC into another group of NEN which is not in accordance with the WHO classification (17) and is also distinct from the classification suggested by Rindi et al. (11). Rindi et al. (11) included information on findings by SSR scintigraphy in 3 patients with TC and 5 patients with AC, and found a higher incidence of negative scans in TC as compared to AC (33% vs. 20%). Our observation that the proliferation rates of TC and AC metastases were significantly higher than those of the primaries shows that we cannot generalise and transfer the results for SUVmax of SSR PET in primary tumors to its metastases (18).

The diagnostic challenges imposed due to complex inter- and intrapatient differences in the clonal behaviour of primary tumors and metastases can be overcome by combining different imaging tools. Indeed, in our study only the combination of both functional SSR PET imaging and morphological contrast-enhanced CT imaging yielded the maximum information necessary for appropriate staging and restaging because concordant results between SSR PET and CT were observed in only 54% of the lesions.

In general, in our patient cohort, CT was more sensitive for staging of liver and lung lesions whereas PET performed significantly better in the detection of bone metastases. Lower sensitivity of PET in the detection of lung lesions as well as liver lesions as

compared to CT is at least partly be attributable to the partial volume effect in lesions below 1 cm in diameter, the normal physiological uptake of ^{68}Ga-DOTATOC / DOTATATE in liver tissue as well as to breathing movement artefacts (19). Nevertheless, in patients referred for restaging, additional findings on PET lead to upstaging with a relevant change in management strategy in approximately every fifth patient.

Surgery is generally offered with curative intent to all patients with operable well-differentiated metastases from NET regardless of the site of origin (foregut, midgut or hindgut) (20). The majority of patients will have recurrent disease within 5 years if distant metastases were present at initial diagnosis (20). One of the patients in our retrospective analysis presented with local recurrence 10 years after the first surgical resection. Late occurrence of metastases in patients with carcinoid lung tumors has been already previously reported and necessitates regular follow-up of such patients for at least 10 years (21) and probably for their whole life.

The frequency and interval of following up such patients with PET/CT can easily be determined if NETtest, a non-invasive method, is used to determine the presence or absence of disease. We have shown that NETest is positive in all the patients with positive SSR PET/CT. Not only that, specific transcripts can predict the presence of somatostatin receptor expression density as measured by SUVmax making it a very useful tool to pre-select patients for imaging with SSR PET/CT or FDG PET/CT. By combining SUVmax with MOR4FL2 it is possible to generate another risk parameter to predict disease progression and thus, indicate early alternative treatment intervention.

The treatment strategy of LNETs also depends on their potential to metastasise. Our observation, that TC metastasises less frequently as compared to AC is in line with previous studies: this difference is related to their differences in proliferative activity and, thus, aggressiveness, with AC having a higher frequency of nodal (50%) and distant metastases (20%) as compared to TC (21,22). However, typical carcinoids can also metastasize as shown in our retrospective analyses in which PET/CT revealed metastases in 50% of the patients, making it mandatory to perform SSR PET/CT in patients with TC at least once for staging and restaging to rule out distant metastases.

On the other side of the spectrum of lung neuroendocrine neoplasms, as far as receptor expression and mismatch between SSR PET and CT results is concerned, are the DIPNECH. Management of patients with DIPNECH has always posed a major challenge because very little is known about their exact biological behaviour and clinical course (24,25). In our analysis, we identified three patients with malignant transformation of initial DIPNECH into TC or AC. One of these patients also developed lymph node metastases and later on responded to chemotherapy underscoring the need of routine follow-up in this rare type of lung tumors.

6. Limitations

The major limitation of all the results analysed and discussed are a) the retrospective nature of the study design, b) the low number of LNET patients due to the rarity of this entity, c) the use of three SSR tracers with somewhat different although clinically not relevant somatostatin receptor affinities d) the use of different PET scanners which might influence SUV measurement, and e) last but not the least an institutional bias which might have a strong influence on the results specially with respect to the role of SSR PET in LNET. These challenges can be overcome in the future by prospective multicentre studies organised at ENETS centres of excellence in NET.

7. Summary

We could show that SUVmax is significantly correlated to SSR density in various NET entities as measured by manual and digital immunohistochemistry and, thus, can be used for prediction of SSR expression on NET tumor lesions. These results validate maximum Standardized Uptake Value (SUVmax) on SSR PET/CT, using either ^{68}Ga-DOTATOC, ^{68}Ga-DOTATATE or ^{68}Ga-DOTANOC, as a reliable semiquantitative imaging parameter for the density of somatostatin receptor expression on tumor lesions.

NETest, analysing the NET transcript signature, appears to be an interesting non-invasive blood test which was significantly correlated with SSR PET positivity, and can be used to predict SSR PET/CT based SUVmax.

Based on these correlations of SUVmax with tumor characteristic SSR expression, the application of SSR PET/CT for characterization of lung NET tumors revealed that typical and atypical lung carcinoid patients have different and complex patterns of metastases with variable SSR expression. Because SSR PET in addition to CT had significant impact on the treatment strategy in up to 23% of patients with typical and atypical lung carcinoids, it seems necessary to combine functional SSR PET and contrast-enhanced CT for appropriate restaging in LNET patients.

8. References

1. Reubi JC, Waser B. Concomitant expression of several peptide receptors in neuroendocrine tumours: molecular basis for in vivo multireceptor tumour targeting. Eur J Nucl Med Mol Imaging. 2003 May;30(5):781-93

2. Bodei L, Sundin A, Kidd M, **Prasad V**, Modlin IM. The status of neuroendocrine tumor imaging: from darkness to light? Neuroendocrinology. 2015;101(1):1-17

3. Kidd M, Drozdov I, Modlin I Blood and tissue neuroendocrine tumor gene cluster analysis correlate, define hallmarks and predict disease status. Endocr Relat Cancer. 2015 Aug;22(4):561-75

4. Daniel K, Maria A, Amelie L, Isabell L, Stefan S, Luisa P, Merten H, **Vikas P**, Gerd B, Paul BR, Somatostatin receptor immunohistochemistry in neuroendocrine tumors: comparison between manual and automated evaluation. Int J Clin Exp Pathol. 2014 Jul 15;7(8):4971-80 (authors name in pubmed are arranged according to the first name)

5. Virgolini I, Ambrosini V, Bomanji JB, Baum RP, Fanti S, Gabriel M, Papathanasiou ND, Pepe G, Oyen W, De Cristoforo C, Chiti A. Procedure guidelines for PET/CT tumour imaging with 68Ga-DOTA-conjugated peptides: 68Ga-DOTA-TOC, 68Ga-DOTA-NOC, 68Ga-DOTA-TATE. Eur J Nucl Med Mol Imaging. 2010 Oct;37(10):2004-10.

6. Bodei L, Kidd M, Modlin IM, **Prasad V**, Severi S, Ambrosini V, Kwekkeboom DJ, Krenning EP, Baum RP, Paganelli G, Drozdov I Gene transcript analysis blood values correlate with ^{68}Ga-DOTA-somatostatin analog (SSA) PET/CT imaging in neuroendocrine tumors and can define disease status. Eur J Nucl Med Mol Imaging. 2015 Aug;42(9):1341-52

7. Friedman J, Hastie T, and Tibshirani R. Regularization Paths for Generalized Linear Models via Coordinate Descent. J Stat Soft. 2010;33(1):1-22.

8. Kuhn M. Building Predictive Models in R Using the caret Package. J Stat Soft. 2008;28(5):1-26.

9. Hanley JA, and McNeil BJ. The meaning and use of the area under a receiver operating characteristic (ROC) curve. Radiology. 1982;143(1):29-36.

10. **Prasad V**, Steffen IG, Pavel M, Denecke T, Tischer E, Apostolopoulou K, Pascher A, Arsenic R, Brenner W. Somatostatin receptor PET/CT in restaging of typical and atypical lung carcinoids. EJNMMI Res. 2015 Dec;5(1):53.

11. Rindi G, Klersy C, Inzani F, Fellegara G, Ampollini L, Ardizzoni A et al. Grading the neuroendocrine tumors of the lung: an evidence-based proposal. Endocr Relat Cancer. 2014;21(1):1-16.

12. Bini A, Grazia M, Stella F, Petrella F, Sellitri F, Fanti S et al. The role of somatostatin receptor scintigraphy (Octreoscan) during follow-up of patients after bronchial carcinoid resection. A prospective study. J Cardiovasc Surg (Torino). 2005;46(3):318-9.

13. Kaemmerer D, Wirtz RM, Fischer EK, Hommann M, Sänger J, **Prasad V**, Specht E, Baum RP, Schulz S, Lupp A. Analysis of somatostatin receptor 2A immunohistochemistry, RT-qPCR, and in vivo PET/CT data in patients with pancreatic neuroendocrine neoplasm. Pancreas. 2015 May;44(4):648-54.

14. Kayani I, Conry BG, Groves AM, Win T, Dickson J, Caplin M et al. A comparison of 68Ga-DOTATATE and 18F-FDG PET/CT in pulmonary neuroendocrine tumors. J Nucl Med. 2009;50(12):1927-32.

15. Venkitaraman B, Karunanithi S, Kumar A, Khilnani GC, Kumar R. Role of (68)Ga-DOTATOC PET/CT in initial evaluation of patients with suspected bronchopulmonary carcinoid. Eur J Nucl Med Mol Imaging. 2014;41(5):856-64.

16. Jindal T, Kumar A, Venkitaraman B, Meena M, Kumar R, Malhotra A et al. Evaluation of the role of [18F]FDG-PET/CT and [68Ga]DOTATOC-PET/CT in differentiating typical and atypical pulmonary carcinoids. Cancer imaging. 2011;11:70-5.

17. Brambilla E, Travis WD, Colby TV, Corrin B, Shimosato Y. The new World Health Organization classification of lung tumours. Eur Respir J. 2001;18(6):1059-68.

18. Yokota J. Tumor progression and metastasis. Carcinogenesis. 2000;21(3):497-503.

19. Kuehl H, Veit P, Rosenbaum SJ, Bockisch A, Antoch G. Can PET/CT replace separate diagnostic CT for cancer imaging? Optimizing CT protocols for imaging cancers of the chest and abdomen. J Nucl Med. 2007;48 Suppl 1:45S-57S.

20. Pavel M, Baudin E, Couvelard A, Krenning E, Oberg K, Steinmuller T et al. ENETS Consensus Guidelines for the management of patients with liver and other distant metastases from neuroendocrine neoplasms of foregut, midgut, hindgut, and unknown primary. Neuroendocrinology. 2012;95(2):157-76.

21. Ferolla P, Daddi N, Urbani M, Semeraro A, Ribacchi R, Giovenali P et al. Tumorlets, multicentric carcinoids, lymph-nodal metastases, and long-term behavior in bronchial carcinoids. J Thorac Oncol.. 2009;4(3):383-7.

22. Fink G, Krelbaum T, Yellin A, Bendayan D, Saute M, Glazer M et al. Pulmonary carcinoid: presentation, diagnosis, and outcome in 142 cases in Israel and review of 640 cases from the literature. Chest. 2001;119(6):1647-51.

23. Scott WJ. Surgical treatment of other bronchial tumors. Chest Surg Clin N Am. 2003;13(1):111-28.

24. Davies SJ, Gosney JR, Hansell DM, Wells AU, du Bois RM, Burke MM et al. Diffuse idiopathic pulmonary neuroendocrine cell hyperplasia: an under-recognised spectrum of disease. Thorax. 2007;62(3):248-52.

25. Gorshtein A, Gross DJ, Barak D, Strenov Y, Refaeli Y, Shimon I et al. Diffuse idiopathic pulmonary neuroendocrine cell hyperplasia and the associated lung neuroendocrine tumors: clinical experience with a rare entity. Cancer. 2012;118(3):612-9.

Eidesstattliche Versicherung

„Ich, Vikas Prasad, versichere an Eides statt durch meine eigenhändige Unterschrift, dass ich die vorgelegte Dissertation mit dem Thema: [Somatostatin receptor PET/CT in the management of patients with neuroendocrine tumors] selbstständig und ohne nicht offengelegte Hilfe Dritter verfasst und keine anderen als die angegebenen Quellen und Hilfsmittel genutzt habe.

Alle Stellen, die wörtlich oder dem Sinne nach auf Publikationen oder Vorträgen anderer Autoren beruhen, sind als solche in korrekter Zitierung (siehe „Uniform Requirements for Manuscripts (URM)" des ICMJE -*www.icmje.org*) kenntlich gemacht. Die Abschnitte zu Methodik (insbesondere praktische Arbeiten, Laborbestimmungen, statistische Aufarbeitung) und Resultaten (insbesondere Abbildungen, Graphiken und Tabellen) entsprechen den URM (s.o) und werden von mir verantwortet.

Meine Anteile an den ausgewählten Publikationen entsprechen denen, die in der untenstehenden gemeinsamen Erklärung mit dem/der Betreuer/in, angegeben sind. Sämtliche Publikationen, die aus dieser Dissertation hervorgegangen sind und bei denen ich Autor bin, entsprechen den URM (s.o) und werden von mir verantwortet.

Die Bedeutung dieser eidesstattlichen Versicherung und die strafrechtlichen Folgen einer unwahren eidesstattlichen Versicherung (§156,161 des Strafgesetzbuches) sind mir bekannt und bewusst."

_____

Datum   Unterschrift

Anteilserklärung an den erfolgten Publikationen

Vikas Prasad hatte folgenden Anteil an den folgenden Publikationen:

Publikation 1: **Prasad V**, Steffen IG, Pavel M, Denecke T, Tischer E, Apostolopoulou K, Pascher A, Arsenic R, Brenner W. Somatostatin receptor PET/CT in restaging of typical and atypical lung carcinoids. EJNMMI Res. 2015 Dec;5(1):53.

Beitrag im Einzelnen: 1. Teilnahme an der Konzeption der Studie. 2. Erstellung des Datenblatts. 3. Statistische Analyse der Daten 4. PET/CT Auswertung 5. Teilnahme an der Dateninterpretation 6. Entwurf des Manuskripts.

Publikation 2: Daniel Kaemmerer, Maria Athelogou, Amelie Luppe, Isabell Lenhardt, Stefan Schulz, Luisa Peter, Merten Hommann, **Vikas Prasad**, Gerd Binig, Paul Richard Baum. Somatostatin receptor immunohistochemistry in neuroendocrine tumors: comparison between manual and automated evaluation. Int J Clin Exp Pathol. 2014 Jul 15;7(8):4971-80. (Authors name in pubmed are arranged according to the first name)

Beitrag im Einzelnen: 1. Teilnahme an der Konzeption der Studie. 2. PET/CT Auswertung. 3. Teilnahme an der Dateninterpretation. 4. Entwurf des Manuskripts.

Publikation 3: Bodei L, Kidd M, Modlin IM, **Prasad V**, Severi S, Ambrosini V, Kwekkeboom DJ, Krenning EP, Baum RP, Paganelli G, Drozdov I Gene transcript analysis blood values correlate with ^{68}Ga-DOTA-somatostatin analog (SSA) PET/CT imaging in neuroendocrine tumors and can define disease status. Eur J Nucl Med Mol Imaging. 2015 Aug;42(9):1341-52

Beitrag im Einzelnen: 1. Teilnahme an der Konzeption der Studie. 2. Erstellung des Datenblatts. 3. PET/CT Auswertung. 4. Teilnahme an der Dateninterpretation 5. Entwurf des Manuskripts.

Unterschrift, Datum und Stempel des betreuenden Hochschullehrers/der betreuenden Hochschullehrerin

_____

Unterschrift des Doktoranden/der Doktorandin

_____

Original Article
Somatostatin receptor immunohistochemistry in neuroendocrine tumors: comparison between manual and automated evaluation

Kaemmerer Daniel[1]*, Athelogou Maria[5]*, Lupp Amelie[2]*, Lenhardt Isabell[2], Schulz Stefan[2], Peter Luisa[1], Hommann Merten[1], Prasad Vikas[3,5], Binnig Gerd[4], Baum Richard Paul[5]

[1]Department of General and Visceral Surgery, Zentralklinik Bad Berka, Bad Berka, Germany; [2]Department of Pharmacology and Toxicology, Jena University Hospital, Jena, Germany; [3]Department of Nuclear Medicine, University Hospital Charité Berlin, Germany; [4]Definiens AG, Munich, Germany; [5]Department of Molecular Radiotherapy and Molecular Imaging, Center for PET, Zentralklinik Bad Berka, Bad Berka, Germany. *Equal contributors.

Abstract: Background: Manual evaluation of somatostatin receptor (SSTR) immunohistochemistry (IHC) is a time-consuming and cost-intensive procedure. Aim of the study was to compare manual evaluation of SSTR subtype IHC to an automated software-based analysis, and to in-vivo imaging by SSTR-based PET/CT. Methods: We examined 25 gastroenteropancreatic neuroendocrine tumor (GEP-NET) patients and correlated their in-vivo SSTR-PET/CT data (determined by the standardized uptake values SUVmax,-mean) with the corresponding ex-vivo IHC data of SSTR subtype (1, 2A, 4, 5) expression. Exactly the same lesions were imaged by PET/CT, resected and analyzed by IHC in each patient. After manual evaluation, the IHC slides were digitized and automatically evaluated for SSTR expression by Definiens XD software. A virtual IHC score "BB1" was created for comparing the manual and automated analysis of SSTR expression. Results: BB1 showed a significant correlation with the corresponding conventionally determined Her2/neu score of the SSTR-subtypes 2A (r_s: 0.57), 4 (r_s: 0.44) and 5 (r_s: 0.43). BB1 of SSTR2A also significantly correlated with the SUVmax (r_s: 0.41) and the SUVmean (r_s: 0.50). Likewise, a significant correlation was seen between the conventionally evaluated SSTR2A status and the SUVmax (r_s: 0.42) and SUVmean (r_s: 0.62). Conclusion: Our data demonstrate that the evaluation of the SSTR status by automated analysis (BB1 score), using digitized histopathology slides ("virtual microscopy"), corresponds well with the SSTR2A, 4 and 5 expression as determined by conventional manual histopathology. The BB1 score also exhibited a significant association to the SSTR-PET/CT data in accordance with the high affinity profile of the SSTR analogues used for imaging.

Keywords: Somatostatin receptor, molecular imaging, immunohistochemistry, neuroendocrine tumor, PET/CT

Introduction

Neuroendocrine tumors (NET) are an extremely heterogeneous group of neoplasms. Therefore, the diagnostics and therapy are significantly influenced by various biological properties, such as degree of differentiation (grading), tumor proliferation (e.g., Ki-67 index) and staging [1-3].

Somatostatin receptors (SSTR) are expressed in nearly all neuroendocrine tumors (NET), especially in gastroenteropancreatic NET (GEP-NET). There are 5 human SSTR subtypes known (SSTR1, 2A, 3, 4, 5), which in a variable pattern and density are all expressed in GEP-NET. In

GEP-NET, the diagnostics and treatment of each individual patient is based on the SSTR expression profile of the respective tumor [4]. SSTR serve as the molecular basis for high sensitive molecular imaging procedures (PET/CT) as well as therapy targets for long-acting somatostatin receptor analogues and peptide receptor-radionuclide therapy (PRRT) [5, 6]. The maximum - and mean standardized uptake values (SUVmax, SUVmean) in SSTR-based PET are directly associated to the used peptide. These synthetic SSTR-analogues are characterized by a different SSTR-affinity profile to each SSTR-subtype [7]. As shown by Ocak et al. the clinical images with different peptides gave comparable results but the SUVvalues differ significantly

Table 1. Patients characteristic

Number	Age	Sex	Primary tumor	Grading	Origin of lesions
1	69	male	CUP	2	I Liver - MTS
2	71	female	Duodenum	2	I Peritoneal - MTS
3	43	male	Appendix	3	I Appendix - PT
					II Peritoneal - MTS
4	70	male	Ileum	2	I Liver - MTS
5	43	female	Ileum	2	I Lymph node - MTS
6	73	male	Ileum	2	I Liver - MTS
7	51	male	Ileum	2	I Ileum - PT
8	33	female	Pancreas	2	I Pancreas - PT
9	51	male	Pancreas	2	I Meso - MTS
10	57	female	Pancreas	2	I Liver - MTS
11	48	female	Pancreas	2	I Liver - MTS
12	82	male	Ileum	2	I Meso - MTS
					II Meso - MTS
					III Ileum - PT
					IV Peritoneal - MTS
13	49	male	Stomach	2	I Liver - MTS
14	65	female	Pancreas	2	I Liver - MTS
15	59	female	Pancreas	2	I Pancreas - PT
16	54	male	Ileum	1	I Liver - MTS
					II Ileum - PT
17	71	male	Pancreas	2	I Small-intestine - MTS
18	52	female	Ileum	2	I Peritoneal - MTS
19	77	male	Pancreas	2	I Stomach - MTS
20	50	male	Ileum	1	I Meso - MTS
					II Lymph node - MTS
21	53	female	Ileum	1	I Ileum - PT
22	73	male	Pancreas	2	I Peritoneal - MTS
23	59	male	Pancreas	1	I Thyroid - MTS
24	45	male	Stomach	3	I Stomach - PT
25	68	female	Ileum	2	I Liver - MTS

Abbreviations: CUP - carcinoma of unknown primary; PT - primary tumor; MTS - metastases.

[8]. The SSTR subtypes distribution and frequency of each tumor lesion are directly connected to uptake in PET and further medical treatment.

Immunohistochemistry is currently the routine standard method for assessing the extent of SSTR subtypes expression in NET cells. Evaluation of the amount of expression is done visually by means of different semiquantitative scoring systems, as e.g. the human epidermal growth factor receptor 2 (HER2/neu) score and the immunoreactive score (IRS). However, still none of this scoring systems has become established as shown by our group in previous

studies, making it difficult to compare different immunohistochemical studies [9]. Immunohistochemical evaluation is a time-consuming, personnel- and cost-intensive process. Furthermore, the evaluation is semiquantitative, poorly standardised and inter-observer biased. Since few years, automated cellular imaging systems are available to improve histopathological investigations [10]. Automatic measurement of cell proliferation and immunohistochemical markers, automated vessel identification in immunohistochemical sections, automated in-situ hybridization (ISH) and semiautomated image analysis of tissue microarrays (TMAs) are performed in workflows already [11-15]. Studies have shown that automated procedures are objective, fast and reproducible with high levels of accuracy and strong correlations of results between manually and automated analysis procedures [16]. Particularly in large clinical trials they have a proven precision, are less observer dependent and have shown a better reproducibility of data than manual methods [17, 18].

Especially for the diagnosis, therapy and prognosis of NET, it is essential to generate objective and quantitative, but also concordant data with the different methods used. However, the extent of correlation between the different modalities used for patient diagnosis and individual therapy has not been quantified so far. In order to achieve such quantifications, we correlated different data sets from different modalities (PET/CT and histopathological data) from the same patient. We quantified tissue morphology, staining distribution and intensity of staining, using both automated image analysis and manually performed Her2/neu and IRS scoring. In a next step, we computed correlations between image analysis results and manual Her2/neu
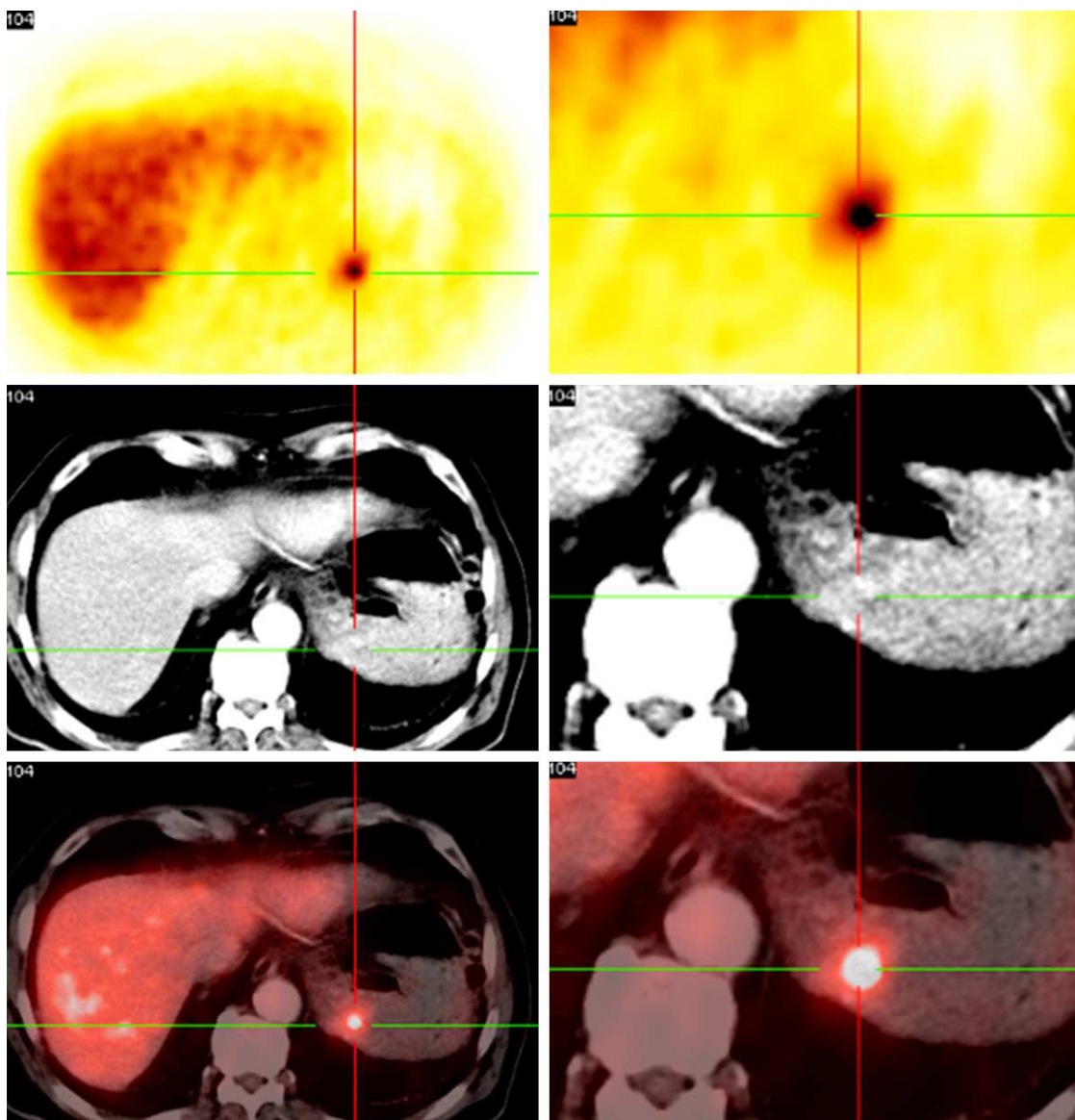
Figure 1. ^{68}Ga-DOTA-NOC PET/CT demonstrates a gastric metastasis of a neuroendocrine pancreatic tumor. The metastasis corresponds with the immunohistochemical image in **Figure 2**.

and IRS scoring. In the present study, for the first time, we present correlations between molecular imaging of SSTR using PET/CT data (SUV max and SUVmean) and immunohistochemical data of SSTR (1, 2A, 4, 5) expression in comparison to an automated image analysis of digitized slides by Definiens Tissue Studio software.

Patients and methods

Twenty-five neuroendocrine tumor patients (**Table 1**) were routinely advised to a surgical procedure by an interdisciplinary tumor board.

All patients signed an informed consent and the study was approved by a local ethics committee. Retrospectively, we obtained PET/CT imaging data from these 25 randomly selected neuroendocrine tumor patients. The patients had received an injection of Ga-68 DOTANOC (n = 17) or DOTATATE (n = 8), which are Gallium-68-radiolabeled analogues of somatostatin and are used in conjunction with PET to image neuroendocrine tumors and their metastases (**Figure 1**). The PET/CTs were routinely performed during the staging process, and Standardized Uptake Values (SUV) as SUVmax and SUVmean of each single tumor lesion were

Table 2. IRS and HER2-scoring system

Percentage of positive cells	X Intensity of Staining	= IRS (0-12)
0 = no positive cells	0 = no colour reaction	0-1 = negative
1 ≤ 10% of positive cells	1 = mild reaction	2-3 = mild
2 = 10-50% positive cells	2 = moderate reaction	4-8 = moderate
3 = 51-80% positive cells	3 = intense reaction	9-12 = strong positive
4 ≥ 80% positive cells		
Her2/neu Score	Reaction Format	Impression
0	No or less than 10% cells	Negative
1+	> 10% cells with minimal staining intensity	Negative
2+	> 10% cells with moderate staining intensity	Mildly positive
3+	> 10% cells with strong staining intensity	Strongly positive

calculated. All patients were examined using a dual-modality PET/CT tomograph (Biograph LSO Duo; Siemens Medical Solutions, U.S.A), as described previously [19]. Patients were then operated and each single tumor lesion (n = 31) was removed, marked and correlated to the lesions, that had already been detected on Ga-68 SSTR PET/CT. Then, immunohistochemical analysis of tumor tissue was performed with specific polyclonal and monoclonal antibodies. The detection of SSTR-subtypes was performed using the labeled streptavidin-biotin-method (LSAB) and counterstaining was done with haematoxylin. The monoclonal rabbit antibody used for detection of SSTR2A was custom produced by Epitomics, Burlingame, CA (USA), and the polyclonal rabbit antibodies for detection of SSTR1, 4 and 5 by Gramsch Laboratories, Schwabhausen (Germany). The rabbit antibodies were generated against the respective carboxyl-terminal tail of each human SSTR-subtype.

The analysis of the stained sections was done with light microscopy according to the immunoreactive score (IRS) by Remmele and Stegner and to the Her2/neu DAKO scoring system as previously described by our group [19, 20] (**Table 2**).

In order to minimize the inter-observer bias, the immunohistochemical analysis was performed by two independent investigators on each tissue section. All immunohistochemically stained slides were digitized using an VS120 slide scanner (Olympus® U.S.A). Then, Definiens software (Definiens Developer XD and Definiens Tissue Studio®; Munich, Germany) was used for the image analysis of the virtual tissue slides. In a first step a simple image analysis

solution was developed and was applied on the virtual slides by using Definiens Developer XD. We used low magnification (5x) of the virtual slides. This first image analysis solution employs chessboard segmentation and threshold classification algorithms for the separation of tissue from non-tissue regions on the slide, assigns tissue regions to different semantic classes according to their stain intensity in "positive", "strong positive" and "negative". "Positive" are stained and "negative" are non-stained tissue regions. Areas of these regions and relations between them are calculated automatically. Such relations are then correlated to Her2- and IRS-score as calculated by the pathologist. In a next step we used Definiens Tissue Studio® (Munich, Germany) for the automated cell-by-cell image analysis and quantification of the virtual slides. Definiens Tissue Studio® identifies regions of interest (ROI) automatically or with learn-by-example approaches, operates through a simple, intuitive user interface and offers unlimited throughput with parallel batch processing. This image analysis solution, separates tumor from non-tumor regions, calculates SSTR (1, 2A, 4, 5) staining intensity in the tumor regions, calculates areas of tumor and non-tumor regions, calculates and quantifies morphological properties of single cells and single cell compartments like nuclei (area, symmetry, staining intensity) and determines relations between tumor and non-tumor regions. Using the image analysis results, the calculation of user defined features in analogy to the HER2/neu score and to the IRS was done.

Similar to the immunoreactive score of Remmele and Stegner, we developed a virtual score "Bad Berka Score 1 (BB1)" which is calcu-

Table 3. Patients data for SSTR2A results and PET/CT data

Patient no./ lesion, slide	IRS SSTR2A	Her2/neu SSTR2A	BB1 SSTR2A	SUVmax	SUVmean
1/1	6	3+	0.4291	5.7	3.4
2/1	3	1+	9.2348	8.2	2.0
3/1	3	1+	N/D	N/D	N/D
3/2	4	1+	0.0906	4.3	2.1
4/1	12	3+	1.0434	13.6	8.1
5/1	9	3+	N/D	6.8	3.9
6/1	12	3+	N/D	33.7	21.0
7/1	4.5	3+	8.9353	8.3	4.9
8/1	12	3+	90.511	25.9	15.8
9/1	4	1+	0.8317	5.7	2.9
10/1	6	3+	4.5260	10.6	6.9
11/1	12	3+	0.9260	5.6	4.6
12/1	4	1+	N/D	N/D	N/D
12/2	12	3+	N/D	4.2	2.7
12/3	12	3+	N/D	N/D	N/D
12/4	12	3+	N/D	4.3	2.8
13/1	6	3+	1.0818	6.4	4.0
14/1	6	3+	4.9974	6.2	4.9
15/1	6	3+	10.024	17.4	10.0
16/1	4.5	3+	0.1238	14.8	9.5
16/2	6	3+	119.52	6.5	3.6
17/1	12	3+	N/D	10.5	6.5
18/1	12	3+	0.8516	12.6	N/D
19/1	12	3+	15.176	9.4	5.5
20/1	9	3+	4.5053	13.5	9.6
20/2	12	3+	14.520	9.6	5.9
21/1	5	3+	7.2947	14.6	9.0
22/1	12	3+	1.9985	12.4	9.1
23/1	12	3+	1.8545	8.4	4.8
24/1	3	1+	0.2441	4.9	2.8
25/1	8	2+	2.7681	6.7	2.0

Abbreviations: N/D - no data available; IRS - Immunoreactive score; Her2/neu - Her2/neu-score; BB1 - digital immunohistochemical score "Bad Berka 1"; SUVmax,-mean standardized uptake value maximum, -mean.

lated by the percentage of cells with high marker intensity multiplied with the mean immunohistochemical marker intensity (BB1 = % cell high marker intensity x mean immunohistochemical marker intensity). In a next step, we used data mining methods in order to find correlations between all the previous data of the same and of different modalities for all patients. 124 immunohistochemical slides from 25 patients were digitized (31 each of the SSTR-subtypes 1, 2A, 4, 5). The SSTR3 slides were not digitized due to logistical problems. From these 124 slides, 23 SSTR1, 23 SSTR2A, 25 SSTR4 and 22 SSTR5 slides were used as virtual slides for the present study. 31 slides of SSTR5 (stained by a new monoclonal anti-SSTR5 antibody) were taken out. All slides were from the same patients who had received the PET/CT scan before (PET/CT data shown in **Table 3**). Most of the patients had more than one tissue sample, sometimes up to five specimens (primary tumor and metastases). We employed Definiens AG Image Analysis (Definiens Tissue Studio®) for the automated analysis of these virtual slides (**Figure 2**). SSTR-stained regions on the slides were assigned as positive and tissue regions without SSTR expression as negative. Regions of interest (ROIs), color intensities, numbers of objects like nuclei and cells and their morphological features among other properties were calculated. Data mining methods were applied in order to quantify correlations between image analysis results of SSTR-stained tissue and the corresponding IRS and HER2/neu scoring data, which have been manually evaluated.

Definiens image analysis technology

The Definiens Software we used for image analysis is based on the Definiens Cognition Network Technology (CNT). The technology is object-oriented, multi-scale, context-driven and knowledge-based [21, 22]. Images are interpreted on the properties of networked image objects, which results in numerous advantages. This approach enables users to bring in detailed expert knowledge and enables complex analyses to be performed with unprecedented accuracy, even on poor quality data or for structures exhibiting heterogeneous properties or variable phenotypes. Extracted structures are the basis for detailed morphometric, structural and relational measurements which can be exported for each individual structure. These data can be used for decision support or correlated against experimental or molecular data. Especially the Definiens Tissue Studio® software enables the user to apply ready to use image analysis solutions in a butch processing
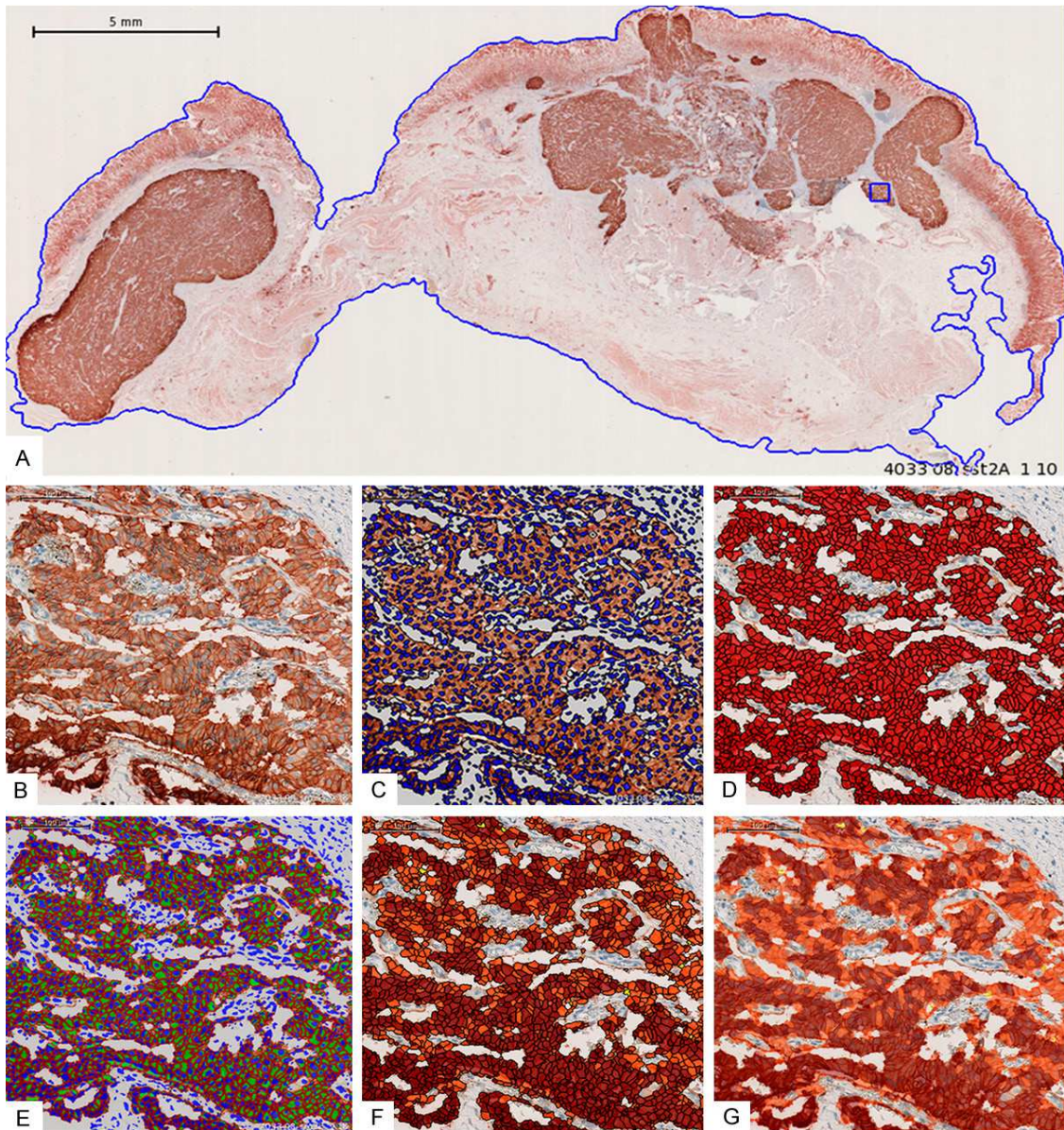
Figure 2. A: Digitized immunohistochemical slide from a gastric metastasis of a neuroendocrine pancreatic tumor showing the selected region of interest (ROI; blue line). The section was stained with a monoclonal antibody against the SSTR2A and displays a strong SSTR2A expression in the tumor cells (brown color; magnification 100 ×). B: Detail of A, showing the predominant localization of the SSTR2A at the plasma membrane of the tumor cells; Initialization of cellular analysis (magnification 600 ×). C: Automated nucleus segmentation (magnification 600 ×). D: Automated cell segmentation (magnification 600 ×). E: Automated cell membrane classification (SSTR2A is a membrane-bound receptor) (magnification 600 ×). F: Automated cell classification according to intensity of cell membrane staining (magnification 600 ×). G: Automated cell classification (transparent) according to plasma membrane staining (magnification 600 ×).

[23, 24]. There are several of such solutions already. These solutions are developed in order to analyze single objects. Single objects are for instance single and their compartments. These image analysis solutions segment and classify individual cells and cell compartments like nuclei, cytoplasm and membranes. So it is possible to classify each individual cell based on the stain of the individual cell membrane, or the stain intensity of the cell cytoplasm, or of the cell nucleus. Visual inspection of the virtual slides showed strong expression of SSTR 1, 4
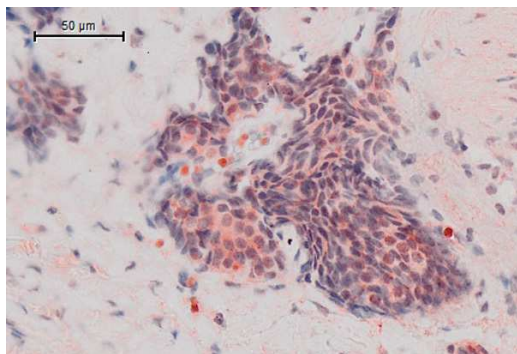
Figure 3. Cytoplasmatic staining of SSTR.

and 5 in the cytoplasm of each individual cell (**Figure 3**). In contrast to SSTR2A, which showed a strong membrane-bound receptor expression (**Figure 2B**). Therefore we used the Tissue Studio® Solutions for classifying each individual cell according to the SSTR expression in the cytoplasm for all these stains. For the SSTR2A we applied the Tissue Studio® Solution, which classifies cells according on the stain in the cell membrane. Both solutions allow the automatically calculation of stain intensity und of morphological properties of each individual object. The results are automatically arranged and are available for further statistical calculations.

Statistical analysis

Statistical analysis was performed using SigmaPlot for Windows Version 11.0, Build 11.0.0.75, Systat Software 2008. Spearman's rank order correlation (r_s) was used to investigate correlations between automated and manually examined immunohistochemical image analysis results (IRS and Her2/neu scoring) and PET/CT uptake values. A *P*-value ≤ 0.05 was considered statistically significant.

Results

The SSTR-subtypes 2A and 5 were mostly confined to the plasma membrane, whereas SSTR1 and SSTR4 were predominantly located in the cytoplasm of the tumor cells. All tumor slides were characterized by a remarkable heterogeneity of staining, both within and between the different samples of the same patient.

Automated analysis of SSTR

The virtual BB1 score was significantly positively correlated (range r_s: 0.43-0.57) to the corre-

sponding manually evaluated IRS and Her2/neu score of the SSTR-subtypes 2A and 5 (**Table 4**). BB1 of SSTR4 only displayed a significant positive correlation with Her2/neu (r_s: 0.44; *P* = 0.028), whereas no significant correlation was seen to IRS (r_s: 0.25; *P* = 0.229). BB1 of SSTR2A exhibited a significant correlation with the SUVmax (r_s: 0.41; *P* = 0.049) and the SUVmean (r_s: 0.50; *P* = 0.019) of the PET/CT. With all other subtypes, SSTR1, SSTR4 and SSTR5, the correlation factor was below 0.1 and no significant correlation was observed (**Table 4**). Separated analysis of patients imaged by DOTA-NOC (n = 16) and DOTA-TATE (n = 8) peptides demonstrated a significant correlation of BB1 of SSTR2A to SUVmax (r_s: 0.58; *P* = 0.018) and SUVmean (r_s: 0.52; *P* = 0.039) whereas no significant correlation was detectable for imaging with DOTA-TATE (Supplementary Tables 1 and 2).

Manually evaluated SSTR data

The SSTR2A expression as evaluated manually by means of the Her2/neu-score was significantly positively correlated to the SUVmax (r_s: 0.42; *P* = 0.028) and SUVmean (r_s: 0.62; *P* < 0.001). In contrast, the SSTR2A expression as determined by the IRS score exhibited no significant correlation to SUVmax (r_s: 0.24; *P* = 0.224) and SUVmean (r_s: 0.34; *P* = 0.081). This was also the case for all other SSTR subtypes (SSTR1, 4, 5) which did not show any significant association to the PET/CT values.

PET/CT data

SUVmax data could be detected in 28/31 lesions with a range from 4.2 to 33.7 (median 8.35). SUVmean data were determined in 27/31 lesions (range 2.0 to 21.0, median 4.9). Some small lesions were not measured or even not detected by molecular imaging but were histologically proven as small metastases.

Discussion

Since few years automated cellular imaging systems are available for improvement of histopathological investigations [10]. In many studies, automatic measurements of cell proliferation and of immunohistochemical markers, automated vessel identification in immunohistochemical sections, automated in-situ hybridization (ISH) and semiautomated image analy-

Table 4. Digital analysis of BB1 in correlation to PET/CT- and manually evaluated immunohistochemical scores

Manual Score / Virtual Score	IRS	Her2/neu	SUVmax (PET/CT data)	SUVmean (PET/CT data)
BB1 (SSTR1)	r: 0.34; *P* = 0.10 N = 24	r: 0.29; *P* = 0.175 N = 24	r: -0.34; *P* = 0.124 N = 22	r: -0.13; *P* = 0.554 N = 21
BB1 (SSTR2A)	r: 0.43; *P* = 0.042* N = 23	r: 0.57; *P* = 0.005* N = 23	r: 0.41; *P* = 0.049* N = 23	r: 0.50; *P* = 0.019* N = 23
BB1 (SSTR4)	r: 0.25; *P* = 0.229 N = 25	r: 0.44; *P* = 0.028* N = 25	r: 0.00; *P* = 0.987 N = 23	r: 0.08; *P* = 0.728 N = 22
BB1 (SSTR5)	r: 0.46; *P* = 0.033* N = 22	r: 0.43; *P* = 0.044* N = 22	r: -0.04; *P* = 0.859 N = 21	r: 0.06; *P* = 0.782 N = 20

Abbreviations: IRS - Immunoreactive score; Her2/neu - Her2/neu-score; BB1 - digital immunohistochemical score "Bad Berka 1"; SUVmax,-mean standardized uptake value maximum, -mean; r: correlation factor; *p < 0.05.

sis of tissue microarrays (TMAs), have been proven to be comparable to manual analysis [11-15]. Additionally, these automated procedures have been shown to be cost-effective and time saving [16]. Particularly in large clinical trials they have a proven precision, are less observer dependent and have shown a better reproducibility of data in comparison to manual ones [17, 18].

However, although many automatic procedures are used during routine histopathology already, quantitative correlations between automated and manually evaluated modalities used for neuroendocrine tumor patients are not available so far.

Previous studies have demonstrated the significant positive association between the SUV of SSTR-based PET/CT and in-vitro immunohistochemical analysis [25, 26]. In the present study, we were also able to detect a significant positive correlation between the SSTR2A expression as evaluated manually according to the Her2/neu score and the PET/CT SUVmax and -mean. However, SSTR2A expression as determined by IRS did not show any significant association to PET/CT data. This latter result is in contradiction to the studies of Miederer and Kaemmerer et al. who were able to demonstrate a strong correlation between SUV in PET/CT and SSTR2A expression [19, 26]. Both of these studies reported data from patients who were injected and analyzed by only one SSTR-analogue (DOTA-TOC or DOTA-NOC), whereas in the present investigation PET/CT data were obtained with two different peptides (DOTA-TATE and DOTA-NOC), displaying quite different SSTR-affinities, were included. DOTA-TATE showed a 10 times higher affinity to SSTR2A than DOTA-NOC [7]. This could be one explanation for our results and for the discrepancy between the two scoring systems.

BB1 was created as a virtual immunohistochemical score. Our data show a significant positive correlation between the BB1 of the SSTR2A, the manually evaluated SSTR2A expression and the SUVmax and SUVmean of the PET/CT. The BB1s of the other SSTRs, in contrast, displayed no correlation to the PET/CT data. With regard to the somatostatin analogues used for the PET/CT measurements in the present investigation, these results seem to be reasonable, because the affinity of these peptides to the SSTR2A is much higher than to all other SSTR subtypes [27]. In the present investigation correlation factors ranging from 0.25 to 0.57 were observed between the BB1 and the corresponding manual data. These correlations were significant for the SSTR2A and the SSTR5 expression both with respect to the IRS and to the Her2/neu scoring system. Concerning the SSTR4 expression, a significant correlation between the BB1 and the respective manual data was seen for the HER2/neu scoring system only.

In clinical practice, in vivo molecular imaging by somatostatin-analogue-based PET/CT has become the golden standard for diagnostics of GEP-NET. To further optimize molecular imaging and to save financial and staff resources, it is useful to evaluate the SSTR subtype status of the tumor beforehand. Without a molecular sstr targets a molecular sstr based imaging procedure is useless. For this, the immunohistochemical evaluation of the SSTR status on formalin-fixed, paraffin-embedded resected tumor specimens has become the method of choice [28, 29]. It is cheaper and faster than autoradiography, does not require radioactive material and can be done during routine histopathological examinations. Our data provide further clinical evidence for the feasibility of an automated evaluation of immunohistochemical stainings e.g. by means of the Definiens soft-

ware tools [17, 18]. Thus, in future, the immuno-histochemical slides can be digitized and analyzed by an automated image analysis procedure to evaluate the SSTR subtype profile prior to further diagnostic and therapeutic recommendations.

Conclusion

In summary, it can be concluded that the evaluation of the main interesting SSTR subtypes (2A and 5) of a given tumor by an automatic SSTR analysis is a reliable method to further improve diagnostics and the assignment of the patients to a stratified therapy with one of the different somatostatin analogues available for PRRT or pharmacological treatment.

Disclosure of conflict of interest

Prof. G. Binnig is founder and Dr. M. Athelogou employee of the company Definiens AG, Munich, Germany. Prof. G. Binning developed Definiens Cognition Network Technology®. All other authors declare no conflicts of interest regarding this manuscript.

Address correspondence to: Dr. Kaemmerer Daniel, Department of General and Visceral Surgery, Zentralklinik Bad Berka GmbH, Robert-Koch-Allee 9 99437 Bad Berka, Germany. Tel: + 49 36458 542701; Fax: + 49 36458 53536; E-mail: Daniel. Kaemmerer@zentralklinik.de

References

[1] Kloppel G and Anlauf M. Epidemiology, tumour biology and histopathological classification of neuroendocrine tumours of the gastrointestinal tract. Best Pract Res Clin Gastroenterol 2005; 19: 507-517.

[2] Kloppel G, Rindi G, Anlauf M, Perren A and Komminoth P. Site-specific biology and pathology of gastroenteropancreatic neuroendocrine tumors. Virchows Arch 2007; 451 Suppl 1: S9-27.

[3] Anlauf M. Neuroendocrine neoplasms of the gastroenteropancreatic system: pathology and classification. Horm Metab Res 2011; 43: 825-831.

[4] Reubi JC. Somatostatin and other Peptide receptors as tools for tumor diagnosis and treatment. Neuroendocrinology 2004; 80 Suppl 1: 51-56.

[5] Baum RP and Kulkarni HR. THERANOSTICS: From Molecular Imaging Using Ga-68 Labeled Tracers and PET/CT to Personalized Radionu-clide Therapy - The Bad Berka Experience. Theranostics 2012; 2: 437-447.

[6] Baum RP, Kulkarni HR and Carreras C. Peptides and receptors in image-guided therapy: theranostics for neuroendocrine neoplasms. Semin Nucl Med 2012; 42: 190-207.

[7] Antunes P, Ginj M, Zhang H, Waser B, Baum RP, Reubi JC and Maecke H. Are radiogallium-labelled DOTA-conjugated somatostatin analogues superior to those labelled with other radiometals? Eur J Nucl Med Mol Imaging 2007; 34: 982-993.

[8] Ocak M, Demirci E, Kabasakal L, Aygun A, Tutar RO, Araman A and Kanmaz B. Evaluation and comparison of Ga-68 DOTA-TATE and Ga-68 DOTA-NOC PET/CT imaging in well-differentiated thyroid cancer. Nucl Med Commun 2013; 34: 1084-1089.

[9] Kaemmerer D, Peter L, Lupp A, Schulz S, Sanger J, Baum RP, Prasad V and Hommann M. Comparing of IRS and Her2 as immunohistochemical scoring schemes in gastroentero-pancreatic neuroendocrine tumors. Int J Clin Exp Pathol 2012; 5: 187-194.

[10] Minot DM, Kipp BR, Root RM, Meyer RG, Reynolds CA, Nassar A, Henry MR and Clayton AC. Automated cellular imaging system III for assessing HER2 status in breast cancer specimens: development of a standardized scoring method that correlates with FISH. Am J Clin Pathol 2009; 132: 133-138.

[11] Alvarenga AW, Coutinho-Camillo CM, Rodrigues BR, Rocha RM, Torres LF, Martins VR, da Cunha IW and Hajj GN. A Comparison between Manual and Automated Evaluations of Tissue Microarray Patterns of Protein Expression. J Histochem Cytochem 2013; 61: 272-282.

[12] Grin A, Brezden-Masley C, Bauer S and Streutker CJ. HER2 In Situ Hybridization in Gastric and Gastroesophageal Adenocarcinoma: Comparison of Automated Dual ISH to FISH. Appl Immunohistochem Mol Morphol 2013; 21: 561-6.

[13] Fiore C, Bailey D, Conlon N, Wu X, Martin N, Fiorentino M, Finn S, Fall K, Andersson SO, Andren O, Loda M and Flavin R. Utility of multispectral imaging in automated quantitative scoring of immunohistochemistry. J Clin Pathol 2012; 65: 496-502.

[14] van der Laak JA, van Engelen N, Melissen M and Hebeda KM. Automated measurement of MIB-1 positive area as an alternative to counting in follicular lymphoma. Cytometry A 2012; 81: 527-531.

[15] Mikalsen LT, Dhakal HP, Bruland OS, Nesland JM and Olsen DR. Quantification of angiogenesis in breast cancer by automated vessel identification in CD34 immunohistochemical sections. Anticancer Res 2011; 31: 4053-4060.

[16] Lopez C, Lejeune M, Salvado MT, Escriva P, Bosch R, Pons LE, Alvaro T, Roig J, Cugat X, Baucells J and Jaen J. Automated quantification of nuclear immunohistochemical markers with different complexity. Histochem Cell Biol 2008; 129: 379-387.

[17] Rohner F, Zeder C, Zimmermann MB and Hurrell RF. Comparison of manual and automated ELISA methods for serum ferritin analysis. J Clin Lab Anal 2005; 19: 196-198.

[18] Fanaian NK, Cohen C, Waldrop S, Wang J and Shehata BM. Epstein-Barr virus (EBV)-encoded RNA: automated in-situ hybridization (ISH) compared with manual ISH and immunohistochemistry for detection of EBV in pediatric lymphoproliferative disorders. Pediatr Dev Pathol 2009; 12: 195-199.

[19] Kaemmerer D, Peter L, Lupp A, Schulz S, Sanger J, Prasad V, Kulkarni H, Haugvik SP, Hommann M and Baum RP. Molecular imaging with 68Ga-SSTR PET/CT and correlation to immunohistochemistry of somatostatin receptors in neuroendocrine tumours. Eur J Nucl Med Mol Imaging 2011; 38: 1659-1668.

[20] Kaemmerer D, Lupp A, Peter L, Fischer E, Schulz S, Kloppel G and Hommann M. Correlation of monoclonal and polyclonal somatostatin receptor 5 antibodies in pancreatic neuroendocrine tumors. Int J Clin Exp Pathol 2013; 6: 49-54.

[21] Baatz M, Zimmermann J and Blackmore CG. Automated analysis and detailed quantification of biomedical images using Definiens Cognition Network Technology. Comb Chem High Throughput Screen 2009; 12: 908-916.

[22] Abraham BK, Fritz P, McClellan M, Hauptvogel P, Athelogou M and Brauch H. Prevalence of CD44+/CD24-/low cells in breast cancer may not be associated with clinical outcome but may favor distant metastasis. Clin Cancer Res 2005; 11: 1154-1159.

[23] Schutze S, Loleit T, Zeretzke M, Bunkowski S, Bruck W, Ribes S and Nau R. Additive microglia-mediated neuronal injury caused by amyloid-beta and bacterial TLR agonists in murine neuron-microglia co-cultures quantified by an automated image analysis using cognition network technology. J Alzheimers Dis 2012; 31: 651-657.

[24] Schonmeyer R, Athelogou M, Sittek H, Ellenberg P, Feehan O, Schmidt G and Binnig G. Cognition Network Technology prototype of a CAD system for mammography to assist radiologists by finding similar cases in a reference database. Int J Comput Assist Radiol Surg 2011; 6: 127-134.

[25] Haug AR, Assmann G, Rist C, Tiling R, Schmidt GP, Bartenstein P and Hacker M. Quantification of immunohistochemical expression of somatostatin receptors in neuroendocrine tumors using 68Ga-DOTATATE PET/CT. Radiologe 2010; 50: 349-354.

[26] Miederer M, Seidl S, Buck A, Scheidhauer K, Wester HJ, Schwaiger M and Perren A. Correlation of immunohistopathological expression of somatostatin receptor 2 with standardised uptake values in 68Ga-DOTATOC PET/CT. Eur J Nucl Med Mol Imaging 2009; 36: 48-52.

[27] Reubi JC, Schar JC, Waser B, Wenger S, Heppeler A, Schmitt JS and Macke HR. Affinity profiles for human somatostatin receptor subtypes SST1-SST5 of somatostatin radiotracers selected for scintigraphic and radiotherapeutic use. Eur J Nucl Med 2000; 27: 273-282.

[28] Fischer T, Doll C, Jacobs S, Kolodziej A, Stumm R and Schulz S. Reassessment of sst2 somatostatin receptor expression in human normal and neoplastic tissues using the novel rabbit monoclonal antibody UMB-1. J Clin Endocrinol Metab 2008; 93: 4519-4524.

[29] Kulaksiz H, Eissele R, Rossler D, Schulz S, Holt V, Cetin Y and Arnold R. Identification of somatostatin receptor subtypes 1, 2A, 3, and 5 in neuroendocrine tumours with subtype specific antibodies. Gut 2002; 50: 52-60.

Supplementary Table 1. Digital analysis of BB1 in correlation to PET/CT- and manually evaluated immunohistochemical scores for patients with DOTA-NOC

Virtual Score \ Manual Score	IRS	Her2/neu	SUVmax (PET/CT data)	SUVmean (PET/CT data)
BB1 (SSTR1)	r: 0.42; *P* = 0.10 N = 16	r: 0.35; *P* = 0.18 N = 16	r: -0.23; *P* = 0.38 N = 16	r: -0.20; *P* = 0.45 N = 16
BB1 (SSTR2A)	r: 0.47; *P* = 0.07 N = 16	r: 0.61; *P* = 0.012* N = 16	r: 0.58; *P* = 0.018* N = 16	r: 0.52; *P* = 0.039* N = 16
BB1 (SSTR4)	r: 0.11; *P* = 0.66 N = 18	r: 0.37; *P* = 0.13 N = 18	r: -0.05; *P* = 0.86 N = 18	r: -0.02; *P* = 0.95 N = 18
BB1 (SSTR5)	r: 0.57; *P* = 0.027* N = 15	r: 0.55; *P* = 0.034* N = 15	r: -0.04; *P* = 0.89 N = 15	r: 0.01; *P* = 0.96 N = 15

r: correlation factor. *: *P* < 0.05.

Supplementary Table 2. Digital analysis of BB1 in correlation to PET/CT- and manually evaluated immunohistochemical scores for patients with DOTA-TATE

Virtual Score \ Manual Score	IRS	Her2/neu	SUVmax (PET/CT data)	SUVmean (PET/CT data)
BB1 (SSTR1)	r: 0.06; *P* = 0.90 N = 8	r: -0.10; *P* = 0.82 N = 8	r: 0.66; *P* = 0.08 N = 8	r: 0.66; *P* = 0.07 N = 8
BB1 (SSTR2A)	r: 0.19; *P* = 0.69 N = 7	r: 0.54; *P* = 0.22 N = 7	r: 0.47; *P* = 0.29 N = 7	r: 0.36; *P* = 0.43 N = 7
BB1 (SSTR4)	r: -0.27; *P* = 0.56 N = 7	r: 0.20; *P* = 0.66 N = 7	r: 0.23; *P* = 0.61 N = 7	r: 0.27; *P* = 0.56 N = 7
BB1 (SSTR5)	r: 0.21; *P* = 0.66 N = 7	r: 0.21; *P* = 0.66 N = 7	r: -0.31; *P* = 0.50 N = 7	r: -0.34; *P* = 0.45 N = 7

r: correlation factor.

1

Bodei L, Kidd M, Modlin IM, **Prasad V**, Severi S, Ambrosini V, Kwekkeboom DJ, Krenning EP, Baum RP, Paganelli G, Drozdov I.

Gene transcript analysis blood values correlate with ^{68}Ga-DOTA-somatostatin analog (SSA) PET/CT imaging in neuroendocrine tumors and can define disease status.

Eur J Nucl Med Mol Imaging. 2015 Aug;42(9):1341-52. doi: 10.1007/s00259-015-3075-9. Epub 2015 May 7.

http:dx.doi.org/10.1007/s00259-015-3075-9

Bodei L, Kidd M, Modlin IM, **Prasad V**, Severi S, Ambrosini V, Kwekkeboom DJ, Krenning EP, Baum RP, Paganelli G, Drozdov I.

Gene transcript analysis blood values correlate with ^{68}Ga-DOTA-somatostatin analog (SSA) PET/CT imaging in neuroendocrine tumors and can define disease status.

Eur J Nucl Med Mol Imaging. 2015 Aug;42(9):1341-52. doi: 10.1007/s00259-015-3075-9. Epub 2015 May 7

http:dx.doi.org/10.1007/s00259-015-3075-9

Bodei L, Kidd M, Modlin IM, **Prasad V**, Severi S, Ambrosini V, Kwekkeboom DJ, Krenning EP, Baum RP, Paganelli G, Drozdov I.

Gene transcript analysis blood values correlate with ^{68}Ga-DOTA-somatostatin analog (SSA) PET/CT imaging in neuroendocrine tumors and can define disease status.

Eur J Nucl Med Mol Imaging. 2015 Aug;42(9):1341-52. doi: 10.1007/s00259-015-3075-9. Epub 2015 May 7

http:dx.doi.org/10.1007/s00259-015-3075-9

Bodei L, Kidd M, Modlin IM, **Prasad V**, Severi S, Ambrosini V, Kwekkeboom DJ, Krenning EP, Baum RP, Paganelli G, Drozdov I.

Gene transcript analysis blood values correlate with ^{68}Ga-DOTA-somatostatin analog (SSA) PET/CT imaging in neuroendocrine tumors and can define disease status.

Eur J Nucl Med Mol Imaging. 2015 Aug;42(9):1341-52. doi: 10.1007/s00259-015-3075-9. Epub 2015 May 7

http:dx.doi.org/10.1007/s00259-015-3075-9

Bodei L, Kidd M, Modlin IM, **Prasad V**, Severi S, Ambrosini V, Kwekkeboom DJ, Krenning EP, Baum RP, Paganelli G, Drozdov I.

Gene transcript analysis blood values correlate with ^{68}Ga-DOTA-somatostatin analog (SSA) PET/CT imaging in neuroendocrine tumors and can define disease status.

Eur J Nucl Med Mol Imaging. 2015 Aug;42(9):1341-52. doi: 10.1007/s00259-015-3075-9. Epub 2015 May 7

http:dx.doi.org/10.1007/s00259-015-3075-9

Bodei L, Kidd M, Modlin IM, **Prasad V**, Severi S, Ambrosini V, Kwekkeboom DJ, Krenning EP, Baum RP, Paganelli G, Drozdov I.

Gene transcript analysis blood values correlate with ^{68}Ga-DOTA-somatostatin analog (SSA) PET/CT imaging in neuroendocrine tumors and can define disease status.

Eur J Nucl Med Mol Imaging. 2015 Aug;42(9):1341-52. doi: 10.1007/s00259-015-3075-9. Epub 2015 May 7

http:dx.doi.org/10.1007/s00259-015-3075-9

Bodei L, Kidd M, Modlin IM, **Prasad V**, Severi S, Ambrosini V, Kwekkeboom DJ, Krenning EP, Baum RP, Paganelli G, Drozdov I.

Gene transcript analysis blood values correlate with ^{68}Ga-DOTA-somatostatin analog (SSA) PET/CT imaging in neuroendocrine tumors and can define disease status.

Eur J Nucl Med Mol Imaging. 2015 Aug;42(9):1341-52. doi: 10.1007/s00259-015-3075-9. Epub 2015 May 7

http:dx.doi.org/10.1007/s00259-015-3075-9

Bodei L, Kidd M, Modlin IM, **Prasad V**, Severi S, Ambrosini V, Kwekkeboom DJ, Krenning EP, Baum RP, Paganelli G, Drozdov I.

Gene transcript analysis blood values correlate with ^{68}Ga-DOTA-somatostatin analog (SSA) PET/CT imaging in neuroendocrine tumors and can define disease status.

Eur J Nucl Med Mol Imaging. 2015 Aug;42(9):1341-52. doi: 10.1007/s00259-015-3075-9. Epub 2015 May 7

http:dx.doi.org/10.1007/s00259-015-3075-9

Bodei L, Kidd M, Modlin IM, **Prasad V**, Severi S, Ambrosini V, Kwekkeboom DJ, Krenning EP, Baum RP, Paganelli G, Drozdov I.

Gene transcript analysis blood values correlate with ^{68}Ga-DOTA-somatostatin analog (SSA) PET/CT imaging in neuroendocrine tumors and can define disease status.

Eur J Nucl Med Mol Imaging. 2015 Aug;42(9):1341-52. doi: 10.1007/s00259-015-3075-9. Epub 2015 May 7

http:dx.doi.org/10.1007/s00259-015-3075-9

Bodei L, Kidd M, Modlin IM, **Prasad V**, Severi S, Ambrosini V, Kwekkeboom DJ, Krenning EP, Baum RP, Paganelli G, Drozdov I.

Gene transcript analysis blood values correlate with ^{68}Ga-DOTA-somatostatin analog (SSA) PET/CT imaging in neuroendocrine tumors and can define disease status.

Eur J Nucl Med Mol Imaging. 2015 Aug;42(9):1341-52. doi: 10.1007/s00259-015-3075-9. Epub 2015 May 7

http:dx.doi.org/10.1007/s00259-015-3075-9

Bodei L, Kidd M, Modlin IM, **Prasad V**, Severi S, Ambrosini V, Kwekkeboom DJ, Krenning EP, Baum RP, Paganelli G, Drozdov I.

Gene transcript analysis blood values correlate with ^{68}Ga-DOTA-somatostatin analog (SSA) PET/CT imaging in neuroendocrine tumors and can define disease status.

Eur J Nucl Med Mol Imaging. 2015 Aug;42(9):1341-52. doi: 10.1007/s00259-015-3075-9. Epub 2015 May 7

http:dx.doi.org/10.1007/s00259-015-3075-9

Bodei L, Kidd M, Modlin IM, **Prasad V**, Severi S, Ambrosini V, Kwekkeboom DJ, Krenning EP, Baum RP, Paganelli G, Drozdov I.

Gene transcript analysis blood values correlate with ^{68}Ga-DOTA-somatostatin analog (SSA) PET/CT imaging in neuroendocrine tumors and can define disease status.

Eur J Nucl Med Mol Imaging. 2015 Aug;42(9):1341-52. doi: 10.1007/s00259-015-3075-9. Epub 2015 May 7

http:dx.doi.org/10.1007/s00259-015-3075-9

EJNMMI Research
a SpringerOpen Journal

ORIGINAL RESEARCH

Open Access

CrossMark

Somatostatin receptor PET/CT in restaging of typical and atypical lung carcinoids

Vikas Prasad[1*], Ingo G. Steffen[1], Marianne Pavel[2], Timm Denecke[3], Elisabeth Tischer[2], Konstantina Apostolopoulou[2], Andreas Pascher[4], Ruza Arsenic[5] and Winfried Brenner[1]

Abstract

Background: To assess the role of somatostatin receptor (SR) PET/CT using Ga-68 DOTATOC or DOTATATE in staging and restaging of typical (TC) and atypical (AC) lung carcinoids.

Methods: Clinical and PET/CT data were retrospectively analyzed in 27 patients referred for staging ($N = 5$; TC, $N = 4$; AC, $N = 1$) or restaging ($N = 22$; TC, $N = 8$; AC, $N = 14$). Maximum standardized uptake value (SUVmax) of SR-positive lesions was normalized to the SUVmax of the liver to generate SUVratio; SR PET was compared to contrast-enhanced (ce) CT. The classification system proposed by Rindi et al. (Endocr Relat Cancer. 2014;21(1):1-16, 2014) was used for classification of patients in TC and AC groups.

Results: Only 18/27 patients were found to have metastases on PET/CT. Of the 186 lesions, 101 (54.3 %) were depicted on both PET and CT, 53 (28.5 %) lesions only on CT, and 32 (17.2 %) only on PET. SUVratio of lesions was significantly higher in AC as compared to TC ($p < 0.001$). In patients referred for restaging, additional findings on PET lead to upstaging with change in management strategy in 5/22 (22.7 %) patients (AC, $N = 5$; TC, $N = 1$). In four patients (all AC) referred for restaging and in one patient (TC) referred for staging, additional findings on CT missed on PET lead to correct staging.

Conclusions: Typical and atypical carcinoid patients have complex patterns of metastases which make it necessary to combine functional SR PET and contrast-enhanced CT for appropriate restaging. In patients referred for restaging SR, PET may have a relevant impact on treatment strategy in up to 22.7 of patients with typical and atypical lung carcinoids.

Keywords: Lung carcinoids; Atypical carcinoid; Typical carcinoid; Somatostatin receptor; PET/CT; Management; Restaging

Background

Neuroendocrine tumors (NET) of the lungs (LNET) represent approximately 30 % of all NET [1, 2] and account for 1–2 % of all lung tumors. According to current WHO classification, LNET are sub-classified into typical carcinoid (TC), atypical carcinoid (AC), and small cell and large cell neuroendocrine carcinoma (LCNEC). TCs are generally low-grade tumors, and ACs are intermediate-grade tumors, whereas the other two entities, small cell lung cancer (SCLC) and LCNEC, are high-grade neoplasms by definition with usually poor prognosis [3]. Of special note

is the fact that up to 10 % of all lung tumors, especially, SCLC show neuroendocrine differentiation [4]. Diffuse idiopathic pulmonary neuroendocrine cell hyperplasia (DIPNECH) without any predisposing conditions has also been reported [5, 6]. DIPNECH is a disease with relatively indolent clinical course, usually remaining stable over several years but with the potential to metastasize in locoregional lymph nodes and rarely to extra thoracic sites [7].

The wide range of histopathological variations of NET with distinct prognosis often poses a clinical challenge not only with respect to the choice of therapy but also to the selection of the appropriate imaging tool for staging and restaging. For small cell lung cancer, the clinical role of F-18-fluoro-deoxyglucose (FDG) PET is well documented for patient management [8]. However, for

* Correspondence: vikas.prasad@charite.de
[1]Department of Nuclear Medicine, Charité Universitätsmedizin, Berlin, Germany
Full list of author information is available at the end of the article

Prasad *et al. EJNMMI Research* (2015) 5:53

Page 2 of 11

the other histological subtypes of lung neuroendocrine neoplasms, there is no general consensus regarding the relative value of CT, MRI (of the liver and spine), and functional imaging with radiolabelled somatostatin analogs for staging and restaging. In specialized centers, patients with low- and intermediate-grade lung carcinoids like TC and AC [9] are usually imaged with somatostatin receptor (SR) scintigraphy or SR PET in addition to the conventional imaging procedures like CT and/or MRI. As yet, however, there has been only one prospective study examining the role of SR scintigraphy during the follow-up of patients after bronchial carcinoid resection [10].

Based on this background, we retrospectively analyzed all TC and AC patients referred to our ENETS Center of Excellence who had undergone both conventional contrast-enhanced CT imaging and SR PET/CT to evaluate if (a) SR PET and/or CT has an impact on the management of TC and AC, (b) to explore the correlation between SUVratio on tumor lesions and the histopathology, i.e., TC and AC, (c) compare SR PET and diagnostic CT in lesion detection, and (d) to look into the role of SR PET/CT in subset of DIPNECH patients.

Methods

Patient selection

Between 1.1.2008 and 13.2.2014, 36 patients with LNET were addressed for somatostatin receptor PET/CT; patients with aggressive LNET (SCLC, $N = 1$; LCNEC, $N = 2$) and those with unknown histopathology (n = 6) were excluded. The remaining 27 patients with histologically proven AC ($n = 15$) and TC ($n = 12$) were included in this retrospective analyses after approval by our local ethics committee (Charité Universitätsmedizin Berlin). All patients were followed up for a minimum of 6 months after the date of PET/CT.

PET/CT was performed in a total of 27 patients (18 females, 9 males) with TC + AC, for restaging after R0 ($N = 20$) and R1 resection ($N = 2$); in 5 patients, SR PET/CT was performed for primary staging purposes. Median age of patients was 63.6 years (range, 33.5–84.1 years). Three patients had secondary tumor manifestations (one patient with ileum NET, one patient with MEN1 syndrome, and one patient with prostate cancer). Patients' characteristics are summarized in Table 1.

Histopathology of lung carcinoids

Internal and external written histopathological reports were reviewed by an experienced pathologist (RA). In unclear or discordant cases, the tumor specimens were re-reviewed by our pathologist (RA) to establish a final diagnosis.

Somatostatin receptor PET/CT

Ga-68 was eluted from Ge-68/Ga-68 generators and labeled either with DOTATATE or DOTATOC according

Table 1 Patients' features: age is given as median/IQR and categorical variables are described by absolute and relative frequencies (%)

Parameter	Patients ($N = 27$)
Age (years)	63.6/53.0–71.0
Gender	
Female	18 (66.7 %)
Male	9 (33.3 %
Histopathology	
TC	12 (44.4 %)
AC	15 (55.6 %)
Initial TNM staging (available for 19 patients)	
T1	9 (47.4 %)
T2	9 (47.4 %)
T3	1 (5.3 %)
N0	15 (78.9 %)
N1	3 (15.8 %)
Nx	1 (5.3 %)
M0	12 (63.2 %)
M1	5 (26.3 %)
Mx	2 (10.5 %)
IASCL stage at initial diagnosis [27] (available for 19 patients)	
Stage Ia	8 (42.1 %)
Stage Ib	5 (26.3 %)
Stage IIa	1 (5.3 %)
Stage IV	5 (26.3 %)
Resection status	
R0	20 (74.1 %)
R1	2 (7.4 %)
Unresected	5 (18.5 %)

to the respective standard labeling procedure already described elsewhere [11]. The selection of either DOTA-TATE or DOTATOC for imaging was purely based on the availability of the compound due to patent regulations. Ga-68-DOTATATE/DOTATOC PET/CT was performed according to the EANM Guidelines [12]. Mean radioactivity injected was 1.7 MBq/Kg of body weight, and the acquisition was performed 45–60 min after the injection of the radiotracer. Until June 2010, PET/CT was performed by a Biograph 16 PET/CT system (Siemens AG, Germany), five to six bed positions each with 3-min acquisition time. After June 2010, all PET scans were acquired in a 3-dimensional acquisition mode on a Gemini TF 16 PET/CT system (Philips Medical Systems) [13]. The standard 3D-LOR algorithm of the system software was used with default parameter settings to reconstruct trans-axial slices of 144×144 voxels with $4.0 \times 4.0 \times 4.0$ mm^3; 10–12 bed positions each with 1.5-min acquisition time;

Prasad *et al. EJNMMI Research* (2015) 5:53

Page 3 of 11

CT was used for the attenuation correction for both the scanners. If contrast-enhanced multi-phase CT was performed at the time of PET/CT ($N = 25$), 70–100 ml Ultravist 370 (Bayer Schering Pharma, Berlin, Germany) with a delay of 30 s for the arterial phase, 50 s for the portovenous phase, and 70 s for venous phase was injected intravenously and images were acquired using bolus tracking methodology, with a collimation of 0.75 mm and a slice thickness of 16×0.75 mm for arterial and portovenous phase whereas for venous phase, slice thickness was 16×1.5 mm. In two patients, contrast-enhanced CT was performed within 4 weeks of PET/CT.

The somatostatin receptor expression in the tumor and normal liver tissue was semi-quantitatively assessed by calculating the maximum standardized uptake value (SUVmax). SUVmax for both the tumor region and the normal liver was determined by using a manual region of interest (ROI) in transaxial attenuation-corrected PET slices. The uptake in the liver was taken as reference value, and the SUVmax of the tumor lesions were normalized internally using SUVmax of the liver for normalization according to the formula normalized uptake in tumor (SUVratio) = SUVmax tumor / SUVmax liver.

SUV were measured only for those lesions which were definitely positive by visual assessment, i.e. the uptake of the lesion was higher than the uptake of the immediate normal surrounding tissue, and which had a size of more than 10 mm in diameter. For bone lesions, size was not taken into consideration according to RECIST criteria. The SUVmax values of Ga-68-DOTATATE/DOTATOC PET/CT can theoretically be influenced by several factors like difference in scanner type, acquisition and reconstruction parameters, and differences in the peptide affinity towards somatostatin receptors among others. For these reasons the normalized values (SUVratio) were preferred over SUVmax for describing the characteristics in the degree of somatostatin receptor expression in both metastases and the primary tumors.

Image analyses

The PET/CT images were analyzed in an interdisciplinary tumor board by experienced and board-certified physicians, primarily by a radiologist (TD), and a nuclear medicine physician (VP). For the image re-evaluation of this study, consensus of the two main readers, nuclear medicine physician (VP), and radiologist (TD) was considered sufficient. In case of discrepancy between these two readers, a second nuclear medicine physician (WB) was involved for a final decision. Data were put in clinical perspective with the pathologist (RA), the attending gastroenterologist (MP), and the surgeon (AP). Lesions seen on PET/CT were characterized as tumor tissue or metastases only if all the physicians achieved a common consensus; in case of any discrepancy between the panelists, lesions were

followed up with CT and/or MRI and by the clinical course. A tracer accumulation on PET images was defined as positive tracer uptake by visual assessment by the two observers VP and TD. Lesions detected only by one modality (CT or PET) were termed positive or negative based on follow-up or complementary imaging modalities like MRI and/or CT. Those patients having both receptor-positive lesions as well as receptor-negative lesions appreciable on CT only were classified as having "mixed lesions".

Statistical analyses

The R-software (version 3.1.3, R Foundation for Statistical Computing, Vienna, Austria) was used for statistical calculations. Categorical variables were analyzed using contingency tables and chi-squared test. If the absolute frequency in contingency table cells was ≤5, Fisher's exact test was used. According to histograms and quantile-quantile plots, a non-parametric distribution of metric variables (SUVmax, SUVratio) was assumed and descriptive parameters are given as median, interquartile range (IQR; 25th quantile-75th quantile), and range (minimum-maximum). Differences between unpaired groups were analyzed using the non-parametric Kruskal-Wallis test (>2 groups) and the Mann-Whitney U test (2 groups), respectively. The association of a metric and a dichotomous variable was analyzed using receiver-operating characteristics (ROC) curves. The optimal cutoff value was defined by the point on the ROC curve with the minimal distance to the point with 100 % sensitivity and 100 % specificity. All tests were performed as two-sided tests, and p values of less than 0.05 were considered as significant.

Results

Histopathology

Patient's histopathology was classified according to the grading system proposed by Rindi et al. [14]. The major difference between the classification proposed by Rindi et al. and the WHO classification is the cutoff value of Ki67.

Based on the Rindi et al. classification, the patient series comprised 12 TC (44.4 %) and 15 AC (55.6 %) patients.

Assessment of Ki67 in tumor tissue (13 PT, 17 metastases) was available in 23 patients (8 TC, 15 AC). In six patients, Ki67 was available from different sites at different time points. The median proliferation rate (Ki67) in metastases (10.0; IQR, 5.0–15.0; $N = 17$) was significantly higher compared to primary tumors (5.0; IQR, 2.0–10.0; $N = 13$) ($p = 0.035$) (see Fig. 1). The median time interval of 31.9 months (IQR, 17.2–44.1) between SR PET and Ki67 evaluation in specimens was relatively long, which could have been partially responsible for the aforementioned significant difference in the Ki67 of metastases and primary tumor.

Prasad *et al. EJNMMI Research* (2015) 5:53

Page 4 of 11
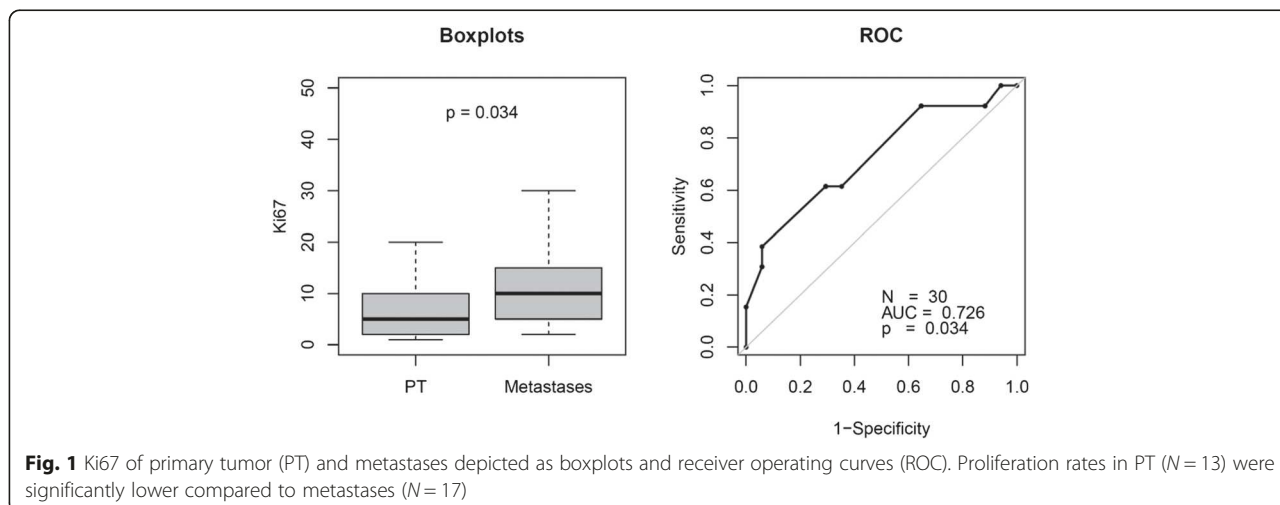
Fig. 1 Ki67 of primary tumor (PT) and metastases depicted as boxplots and receiver operating curves (ROC). Proliferation rates in PT ($N = 13$) were significantly lower compared to metastases ($N = 17$)

Imaging

PET vs. CT—lesion-based analyses

Because of the retrospective nature of the study and ethical issues, none of the discordant lesions were histopathologically confirmed. The discrepant lesions between PET and CT were confirmed by clinical follow-up for at least 6 months and wherever needed also with correlative imaging (CT, MRI, or PET).

Overall, 186 lesions were analyzed: 29 lesions in lungs suspected to be primary tumors ($N = 6$ patients, 3 with multiple lung nodules subclassified as DIPNECH), bone 52, LN 29, liver 49, and other metastases 27. One hundred one lesions (54.3 %) were concordant (both PET and CT visualized the lesions) whereas 53 (28.5 %) lesions were only visible on CT and 32 (17.2 %) lesions were only positive in PET (Table 2). Lesions only positive in PET were significantly more frequent in AC patients ($30/148 = 20.3$ %) compared to TC patients ($2/38 = 5.3$ %, $p = 0.028$).

PET failed to detect 21/29 lung lesions. PET detected 9/49 (18.4 %) additional liver metastases (Table 3), which were not visible on CT. In contrast, CT picked up 23/49 additional liver lesions (46.9 %) not seen on PET

(somatostatin receptor negative). One lesion seen on CT was later on classified as a liver cyst on biopsy. In this patient, all the lesions seen on CT had the same characteristics as the lesion biopsied and therefore were considered as cysts. Two additional lymph nodes (6.9 %) were seen on PET while CT picked up 9/29 (31 %) pathologically enlarged lymph nodes confirmed as metastases by follow-up. CT missed 17/52 bone lesions (32.7 %) whereas PET depicted all 52 bone lesions (results are summarized in Table 2).

SUVmax of SR-positive tumor lesions (133/186) were normalized to the SUVmax of the liver to generate normalized SUV (SUVratio) values. SUVratio was significantly higher in AC (median/IQR/range, 1.7/0.7–2.4/ 0.2–6.4) as compared to TC (median/IQR/range, 0.5/0.3–0.6/0.2–2.6; $p < 0.001$) with respect to all lesions ($N = 133$, PT 8, metastases 125; Fig. 2). AC metastatic lesions (median/IQR/ range, 1.7/0.8–2.4/0.2–6.4) also showed significantly higher SUVratio as compared to TC (median/IQR/range, 0.4/0.3–0.6/0.2–2.0; $p < 0.001$).

PET vs. CT—patient-based analyses

Frequency and characteristics of metastases The frequency of metastases in patients with AC (13/15; 86.7 %) was higher compared to patients with TC with a trend towards significance (6/12; 50 %; $p = 0.087$). In patients with AC, 4/15 had mixed lesions, 3/15 had somatostatin receptor-negative lesions, 2/15 had no detectable lesions on SR PET, whereas in the remaining 6/15, patients all the lesions were somatostatin receptor positive. In patients with TC 1/12 had mixed lesions, 1/12 had PET-negative lesions, 7/12 had no detectable lesions on SR PET, whereas in the remaining three patients, all the lesions were somatostatin receptor positive (Table 4). Frequency of patients with mixed lesions was not statistically significant between TC (1/12 = 8.3 %) and AC (4/15 = 26.7 %; $p =$

Table 2 Absolute and relative frequency of concordant and discordant lesions on PET/CT

	Only positive on PET	Only positive on CT	Concordant positive on PET and CT	Total
PT[a]	0 (0 %)	21(72.4 %)	8 (27.6 %)	29 (15.6 %)
Liver	9 (18.4 %)	23 (46.9 %)	17 (34.7 %)	49 (26.3 %)
Bone	17 (32.7 %)	0 (0 %)	35 (67.3 %)	52 (28.0 %)
Lymph Node	2 (6.9 %)	9 (31.0 %)	18 (62.1 %)	29 (15.6 %)
Others	4 (14.8 %)	0 (0 %)	23 (85.2 %)	27 (14.5 %)
Total	32 (17.2 %)	53 (28.5 %)	101 (54.3 %)	186 (100 %)

[a]3 DIPNECH patients with multiple lung nodules also included

Prasad *et al. EJNMMI Research* (2015) 5:53

Page 5 of 11

Table 3 Patients' characteristics with confirmed liver metastases on CT or PET in follow-up

	Patient 4	Patient 12	Patient 20	Patient 27	Patient 29	Patient 30	Patient 31	Patient 35
Ki67	15 %	10 %	5 %	10 %	1	10 %	20 %	7 %
Histo	AC	AC	AC	AC	TC	AC	AC	AC
Lesion size (mm)	7–32	14–40	20–150	–	–	15–62	21–23	15–19
Somatostatin receptor-positive lung lesions	19/24	0/5	5/5	1/1	2/2	0/7	2/2	2/2
CT-positive lesions	21/24	5/5	4/5	0/1	0/2	7/7	2/2	2/2
SUVmax	7.4–17.4		–	5.2–10.5			16.2–44.4	16.5–17.5

0.34). This was also true analyzing only patients with metastases (TC vs. AC, 1/6 = 16.7 % vs. 4/13 = 30.8 %; $p = 1$).

Bone metastases were present only in AC ($N = 6$) but not in TC patients, and all bone metastases were SR PET-positive lesions.

Effect of PET on management strategy Additional findings on PET missed on CT lead to upstaging in four patients (AC $N = 3$; TC $N = 1$; all restaging) resulting in change in management strategy (Table 5). Two patients (1 AC, 1 TC) with liver metastases but no extrahepatic lesions were treated with transarterial embolization, and afterloading, in one patient (AC), salvage PRRT was ruled out because of stable disease in the bone, and in the fourth patient (AC), a wait-and-watch policy was applied because of low tumor burden.

Fig. 2 Atypical carcinoid lesions showed significantly higher somatostatin receptor expression as compared to typical carcinoid lesions of the lung (SUVmax, $p < 0.05$; SUVratio, $p < 0.001$), SUVmax (**a**) and (**b**); SUVratio (**c**) and (**d**)

Prasad *et al. EJNMMI Research* (2015) 5:53

Page 6 of 11
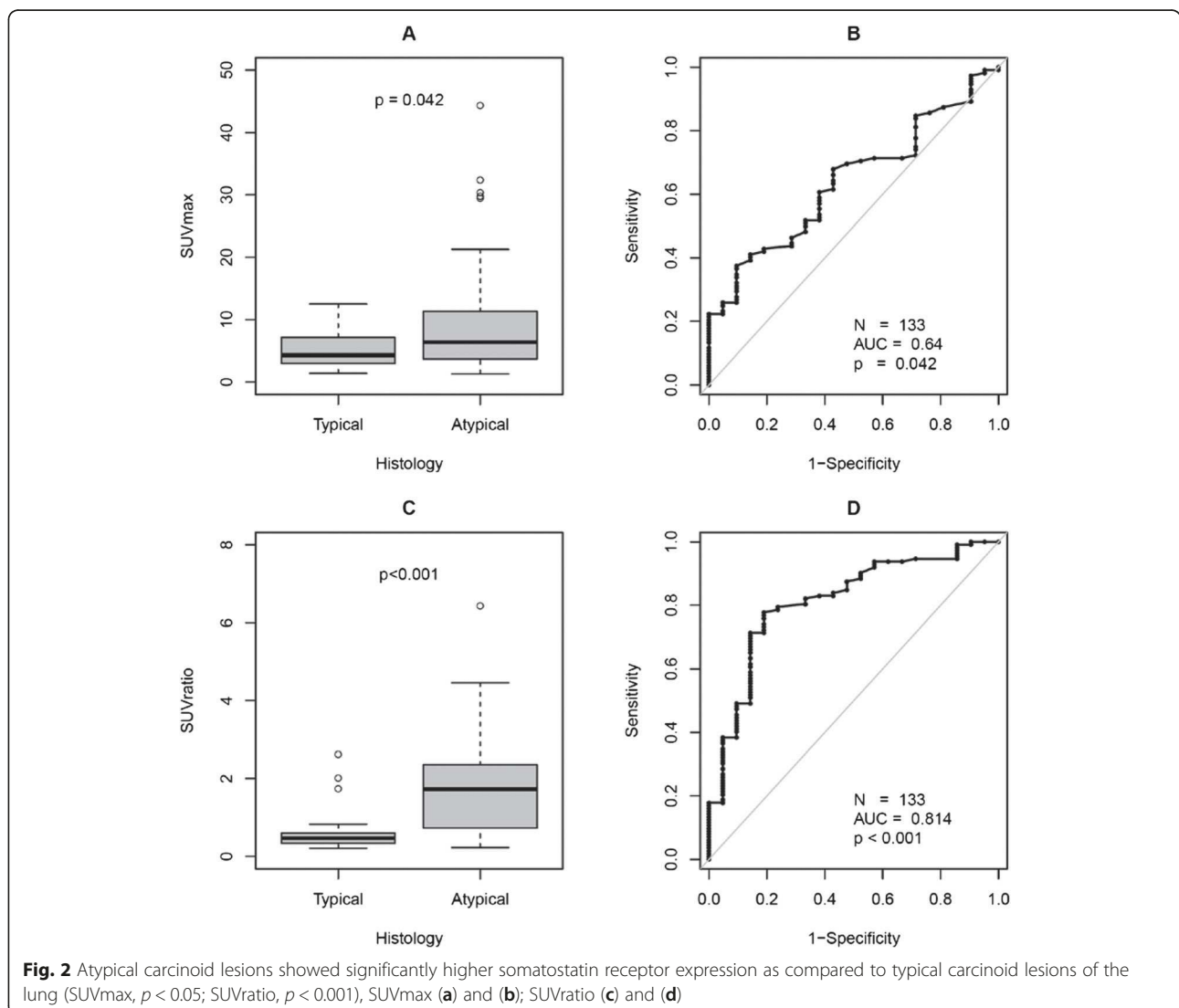
Table 4 Absolute and relative frequency of somatostatin receptor-positive and somatostatin receptor-negative lesions in AC and TC patients

Histopathology	All negative	All positive	Mixed lesions	No metastases	Total
TC	1 (8.3 %)	3 (25 %)	1 (8.3 %)	7 (58.3 %)	12
AC	3 (20.0 %)	6 (40.0 %)	4 (26.7 %)	2 (13.3 %)	15
Total	4 (14.8 %)	9 (33.3 %)	5 (18.5 %)	9 (39.3 %)	27

In four patients referred for restaging (all, AC) and in one patient referred for staging (TC), additional findings on CT missed on PET lead to correct staging (Table 5). In patients referred for restaging, additional findings on PET lead to upstaging with change in management strategy in 4/22 (18.2 %) patients. In one patient (Table 5, patient #8), one of the liver lesions seen on CT was biopsied and was confirmed to be free of malignancy. All the lesions in this patient were found to be somatostatin receptor negative, and the disease was downstaged correctly by PET.

Patients with multiple lung nodules Three of 27 patients (11.1 %) had multiple lung nodules and were subclassified into DIPNECH by the tumor board based on initial findings and the follow-up results. All the lung nodules diagnosed on CT were subclassified as primary tumor due to the absence of histopathological confirmation. One patient presented with nine lymph node metastases all positive on both PET and CT. However, only 6/26 (23.1 %) lung lesions range in size from 6 to 26 mm were found to be somatostatin receptor positive with very low SUVmax (Table 6) in these patients with DIPNECH.

Discussion

The incidence of LNET is increasing [2]. In the absence of evidence-based consensus guidelines on the management of LNET, the current standard of practice varies appreciably according to the availability of diagnostic tools: contrast-enhanced CT is standard in virtually all LNET patients often followed by somatostatin receptor scintigraphy or Ga-68 DOTATOC/DOTATATE PET/CT. There is only one study which prospectively examined the role of SR scintigraphy during the follow-up of patients after bronchial carcinoid resection [10]. Out of 16 patients enrolled, 15 had TC and 1 had AC. The authors compared CT and SR scintigraphy and found SR scintigraphy to be useful in 2/16 patients (12.5 %) whereas CT was found to be of additional benefit to SR scintigraphy in 1/16 patients; on the other hand, SR scintigraphy was found to be false positive due to co-existing sarcoidosis in one patient whereas CT was false positive for a lung nodule in another patient. Although prospective, this study comprised almost only TC patients, and there are no reliable data in AC patients available so far.

This difficulty in standardisation of imaging tools is partly attributable to the rarity as well as to the heterogeneity of LNETs. Although our study presents the results of

Table 5 Patients with PET leading to correct and incorrect staging

Patient ID	Sex	Age	Histo	Ki67	Additional CT information	Additional PET information	Change in management due to PET
PET leading to correct staging							
#27[a]	M	67	AC	2	–	1 liver, 2 bone	SD bone, no salvage PRRT indicated
#8[a]	F	63	AC	3		Liver cysts	Follow-up, without intervention
#28[a]	F	34	AC	15	–	3 bone, 3 others,	Low tumor burden, wait and watch, no PRRT
#29[a]	F	68	TC	5	–	2 liver	Afterloading of liver metastases
#31[a]	F	53	AC	20	–	2 bone	TAE of liver metastases seen on CT and SR PET because of low tumor burden on bone
CT leading to correct staging							
#1[a]	F	74	AC	10	1 recurrent tumor in lung, 9 LN	–	–
#10[b]	F	58	TC	NA	8 PT	–	–
#12[a]	M	59	AC	10	5 liver	1 LN	–
#30[a]	F	50	AC	10	7 liver	–	–

SD stable disease, *LN* lymph nodes, *PT* primary tumor, *TAE* transarterial embolization, *PRRT* peptide receptor radionuclide therapy, *SR* somatostatin receptor, *TC* typical carcinoid, *AC* atypical carcinoid, *M* male, *F* female, *NA* not available
[a]Restaging
[b]Staging

Prasad *et al. EJNMMI Research* (2015) 5:53

Page 7 of 11

Table 6 Characteristics of patients with diffuse pulmonary neuroendocrine cell hyperplasia (DIPNECH)

	Patient 3	Patient 10	Patient 25
Ki67	5 %	NA	15 %
Transformation	TC	TC	AC
Lesion size (mm)	2–18	2–26	2–26
Somatostatin receptor positive lung lesions	4/13	0/8	2/5
SUVmax	1.4–7.9	–	1.0–2.5
LN-Metastases on SR-PET and CT	–	–	9/9

Lesion size and SUVmax are described by minimum-maximum values

somatostatin receptor PET/CT in the largest patient series of low- and intermediate-grade neuroendocrine tumors of the lungs so far, collected over a time period of 6 years, it comprises still a low number of patients with however well-documented histopathology including proliferation rates.

An important aspect of tumor heterogeneity of LNET is the differential somatostatin receptor expression, partially depending on tumor grade. In our study, AC patients with intermediate-grade tumors, although not significant, were found to have a higher proportion of mixed lesions, i.e., both somatostatin receptor-positive and receptor-negative lesions as compared to TC patients which had more homogeneous somatostatin receptor expression. The lack of significance could be because of the relatively low number of patients in the two subgroups as well as due to the lower frequency of metastases in TC as compared to AC. Moreover, in our patient population, proliferation rates of TC and AC metastases were significantly higher than those of the primaries which is partly due to differences between tumor clones in primary tumors and metastases [15] challenging the choice of the perfect tracer for these tumors, i.e., FDG as tracer for rather highly proliferative and high-grade tumors vs. Ga-68-labeled somatostatin receptor analogs, usually considered as tracer of choice for the well-differentiated and, thus, low- and intermediate-grade tumors. These complex inter- and intrapatient differences in the clonal behavior of the primary tumors and the metastases can theoretically be picked up only by combining different imaging tools. Indeed, in our study, only the combination of both functional SR PET imaging and morphological contrast-enhanced CT imaging yielded the maximum information necessary for appropriate staging and restaging because concordant results between SR PET and CT were observed in only 54 % of the lesions. This rather low concordance between both imaging modalities clearly shows the need for combining both with each other to SR PET/contrast-enhanced (ce) CT.

In general, CT was more sensitive for staging of liver and lung lesions whereas PET performed significantly

better in the detection of bone metastases. Lower sensitivity of PET in the detection of lung lesions as well as liver lesions as compared to CT is at least partly be attributable to the partial volume effect below 1 cm in diameter, normal physiological uptake of Ga-68 DOTA-TOC/DOTATATE in liver as well as to breathing movement artefacts [16]. In one patient, the disease in the liver was classified to be polycystic liver disease. In this patient, the hypodense lesions in the liver were all somatostatin receptor negative thereby making it essential to keep this as differential diagnosis in patients with neuroendocrine tumor and somatostatin receptor-negative lesions.

In contrast, additional lesions were detected by PET in 3 AC patients (patient 27, 1 liver lesion, 2 bone lesions; patient 28, 3 lymph node metastases, 3 bone lesions; patient 31, 2 bone lesions) and 1 TC patient (patient 29, 2 liver lesions). More importantly, in patients referred for restaging, additional findings on PET lead to upstaging with change in management strategy approximately every fifth patient.

Apart from allowing correct staging and restaging, combined SR-PET/CT allows selection of appropriate patients for PRRT by ruling out mixed lesions which is a contraindication for performing PRRT and by allowing quantification of somatostatin receptor expression and assessment of SR-positive tumor burden which is required for making a decision on PRRT. In the absence of standardized systemic treatment option for AC and TC patients, PRRT appears to be a valuable therapeutic option. In our overall patient population (data not shown here), three AC patients SR-PET/CT showed very high somatostatin receptor expression and no mismatch between PET and CT results. These patients were treated with PRRT, and an excellent therapy response could be shown in one patient (see Fig. 3).

The treatment strategy of LNETs also depends on their metastasizing potential. Our observation that TC metastasizes less frequently as compared to AC is in line with previous studies: this difference is related to their differences in proliferative activity and, thus, aggressiveness, with AC having a higher frequency of nodal (50 %) and distant metastases (20 %) as compared to TC [17, 18]. However, typical carcinoids can also metastasize as shown in our retrospective analyses in which PET/CT revealed metastases in 50 % of the patients, making it mandatory to perform SR PET/CT in patients with TC at least once for staging/restaging to rule out distant metastases. In the presence of somatostatin receptor-negative lesions during initial staging with SR PET/CT, further follow-up examinations should then be based on clinical symptoms, CT, and serum tumor markers while SR PET/CT should be considered for follow-up examinations in patients with receptor-positive lesions.

For atypical carcinoids, especially in cases with high suspicion of tumor recurrence after surgery and/or higher

Prasad *et al. EJNMMI Research* (2015) 5:53

Page 8 of 11
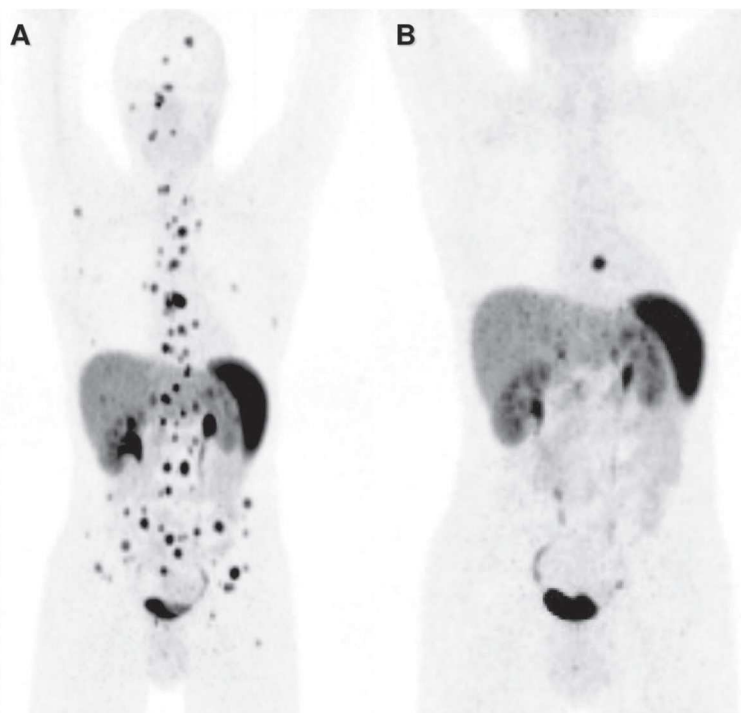
Fig. 3 Atypical carcinoid patient referred for restaging with Ga-68 DOTATOC PET/CT and was treated with 3 cycles of peptide receptor radionuclide therapy (PRRT; 2 cycles of Y-90 DOTATOC and 1 cycle of Lu-177 DOTATATE) showing excellent response. **a** Ga-68 DOTATOC Maximum intensity projection images before PRRT. **b** Ga-68 DOTATOC maximum intensity projection images 22 months after first PRRT

grade tumors, alternatively FDG PET/CT could be performed in case of SR PET-negative lesions as is supported by the study of Kayani et al. [19] who found higher grade LNET to be more FDG avid as compared to Ga-68 DOTATATE. Of special note, they found FDG PET to be less useful in the differentiation of post-radiation changes from vital tumor tissue.

Surgery is generally offered with curative intent to all patients with operable well-differentiated metastases from NET regardless of the site of origin (foregut, midgut, or hindgut) [20]. The majority of patients will have recurrent disease at 5 years if distant metastases were present at initial diagnosis [20]. One of the patients in our retrospective analysis presented with local recurrence 10 years after the first surgical resection (Fig. 4). Occurrence of late metastases in patients with carcinoid lung tumors has been already previously reported and necessitates regular follow-up of such patients for at least 10 years [21] and probably even longer.

Tumor recurrence can either be hepatic and/or extrahepatic. Liver is the most frequent site of distant metastases. Prior to liver surgery with curative intent, it is important to rule out extrahepatic metastases. High rates of detection of bone and lymph node metastases by SR PET suggest that at least one combined SR PET/CT should be performed in patients with AC and TC prior to any liver surgery. However, if liver surgery is planned, MRI with liver-specific contrast

agent should always be performed in addition to CT and/or SR PET/CT because it has the highest sensitivity for detection of liver metastases [22]. One of the inherent limitations of SR PET in detection of liver metastases is the normal physiological uptake of the tracer in hepatocytes which lead to relatively low target non-target ratio, especially if the lesions are smaller than 1 cm or if the lesions have low somatostatin receptor expression.

On the other side of the spectrum of lung neuroendocrine neoplasms, as far as receptor expression and mismatch between SR PET and CT results is concerned, are the DIPNECH. Management of patients with DIPNECH has always posed a major challenge because very little is known about their exact biological behavior and clinical course [5, 7]. In our analysis, we identified three patients with malignant transformation of initial DIPNECH into TC or AC. One of these patients also developed lymph node metastases and later on responded to chemotherapy underscoring the need of routine follow-up in this rare type of lung tumors (Fig. 5).

Our study is not the first one to look into the role of Ga-68-labeled somatostatin receptor PET/CT in LNET. Previous studies have compared Ga-68-DOTATATE and Ga-68-DOTATOC in comparison to FDG PET/CT in patients with AC and TC [19, 23, 24]. In these studies, the main purpose was to look at the different rates of somatostatin receptor expression in TC and AC. We also

Prasad *et al. EJNMMI Research* (2015) 5:53

Page 9 of 11
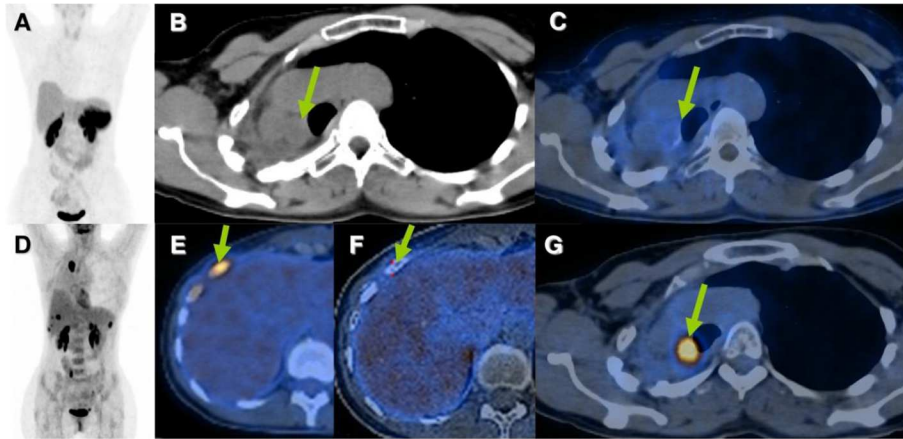
Fig. 4 Atypical carcinoid of the lung, first diagnosed in 03/2000. Following upper and middle lobe resection of the right lung (03/2000) and external beam irradiation therapy with 70 Gy (06/2007), the patient underwent multiple operations for residual tumor. Patient was referred for restaging with Ga-68 DOTATOC and FDG PET/CTs (result not discussed in the text). Both the PET/CTs performed in 2010 showed somatostatin receptor-negative, FDG-positive local residual tumor and bone metastases. **a** Ga-68 DOTATOC PET MIP image. **b** CT axial slides. **c, f** Ga-68 DOTATOC PET/CT fused axial images. **g, e** FDG PET/CT fused axial images. **d** FDG PET MIP image
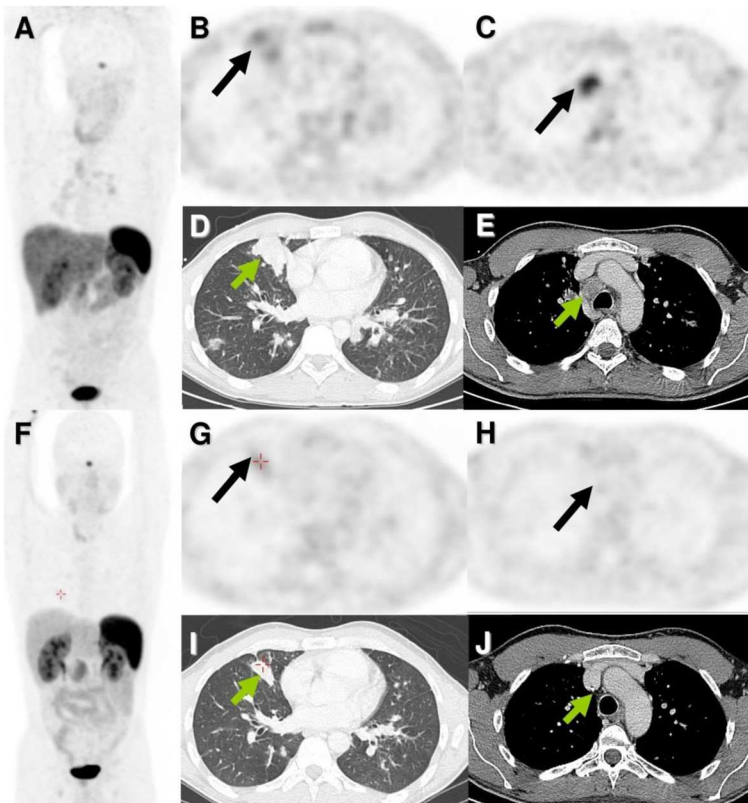
Fig. 5 Patient with initially diffuse pulmonary neuroendocrine cell hyperplasia (DIPNECH) with transformation into an atypical carcinoid was referred for Ga-68 DOTATOC PET/CT. Based on weak somatostatin receptor expression, patients was treated with chemotherapy (folinic acid, 5 fluorouracil, and oxaliplatin) and showed a good response. **a-e** Before chemotherapy. **f-j** After chemotherapy. **a, f** Maximum intensity projection PET images. **b, c, g, h** Axial PET images. **d, e, i, j** Corresponding axial CT images. Partial remission of the mildly receptor positive lesion in the right lung is well appreciated on CT (*arrows*). On MIP images, the previously receptor-positive hilar and mediastinal lymph node lesions also show response to treatment

Prasad *et al. EJNMMI Research* (2015) 5:53

Page 10 of 11

looked at the degree of somatostatin receptor expression in TC and AC. Our findings, however, are contradictory to the previously reported results [19, 23, 24]. In our analysis, TC lesions were found to have a significantly lower tumor SUVmax and SUVratio than AC lesions (Fig. 2) whereas the previously published studies reported significantly higher SUVmax in TC as compared to AC [19, 23, 25]. This difference could be primarily due to the difference in the patient populations. While in our analysis, most of the patients (22/27; 81.5 %) underwent SR PET/CT for restaging after primary tumor resection, in the study from Kayani et al. [19], 83 % (15/18) of the patients underwent SR PET/CT for staging, and the study of Venkitaraman et al. [23] considered only patients ($N = 26$) referred for staging. Furthermore, the ratio of TC (44 %) vs. AC (56 %) in our population is quite different in comparison to Kayani's group [19] with 72 % TC ($N = 11$) vs. 11 % AC ($N = 2$) or Venkitaraman et al. [23] (TC = 81 %, $N = 21$ vs. AC 19 %, $N = 5$). In their analyses of SUV in TC and higher grade LNET, Kayani et al. [19] categorized SCLC and NSCLC with NET differentiation in one group and LCNEC together with AC into another group of NEN which is not in accordance with the WHO classification [4] and is also distinct from the classification suggested by Rindi et al. [14]. Rindi et al. [14] included information on findings by SR scintigraphy in three patients with TC and five patients with AC and found a higher incidence of negative scintigrams in TC as compared to AC (33 % vs. 20 %). Thus, our findings, based on a larger patient population, confirm these initial results by Rindi et al. showing that somatostatin receptor expression is also a valuable biomarker for tumor detection and (re) staging in patients with intermediate grade AC tumors.

One of the major limitations of this analysis is its retrospective nature. Although we included all patients with AC and TC which received SR PET/ceCT at our ENETS center in this analysis, there will probably be a selection bias due to the fact that rather patients with suspicion for relapse or metastatic disease will have been referred for SR PET/CT. Thus, our patient population may not represent the full, i.e., unselected cohort of patients with AC and TC, and thus, the distribution of imaging characteristics of our patients might be biased to some extent. Apart from this, we used in our study both radiotracers, Ga-68 DOTATOC and Ga-68 DOTATATE, for SR PET imaging. The use of either tracer was solely based on its availability due to patent constraints but not on medical reasons. Although these tracers have slightly different binding affinities to somatostatin receptor subtypes, there seems to be no clinically relevant difference in the diagnostic accuracy for NET [20]. However, it would be interesting to also look into other somatostatin receptor analogs covering a broader spectrum of somatostatin receptor subtypes such as Ga-68 DOTANOC [26].

Conclusions

In conclusion, TC and AC patients have complex patterns of metastases which make it necessary to combine functional, i.e., Ga-68 SR PET and morphological imaging, i.e., contrast-enhanced CT for appropriate restaging because only 54 % of the lesions are concordantly detectable by both modalities. The major advantage of SR PET lies in the detection of additional bone lesions. Of similar importance, SR PET/CT allows correct discrimination of patients with heterogeneous (mixed lesions) and homogeneous (all lesions are either somatostatin receptor-positive or somatostatin receptor-negative) lesions which is an essential prerequisite for the selection of the appropriate therapy, especially with respect to PRRT. In patients referred for restaging SR, PET may have a relevant impact on treatment strategy in up to 18 % of patients with typical and atypical lung carcinoids.

Author details
[1]Department of Nuclear Medicine, Charité Universitätsmedizin, Berlin, Germany. [2]Department of Hepatology and Gastroenterology, Charité Universitätsmedizin, Campus Virchow Klinikum, Berlin, Germany. [3]Department of Radiology, Charité Universitätsmedizin, Berlin, Germany. [4]Department of General, Visceral and Transplant Surgery, Charité Universitätsmedizin, Berlin, Germany. [5]Institute of Pathology, Charité Universitätsmedizin, Berlin, Germany.

Prasad *et al. EJNMMI Research* (2015) 5:53

Page 11 of 11

References

1. Gustafsson BI, Kidd M, Modlin IM. Neuroendocrine tumors of the diffuse neuroendocrine system. Curr Opin Oncol. 2008;20(1):1–12.
2. Modlin IM, Lye KD, Kidd M. A 5-decade analysis of 13,715 carcinoid tumors. Cancer. 2003;97(4):934–59.
3. Travis WD, Brambilla E, Müller-Hermelink HK, Harris CC. Pathology andgenetics of tumours of the lung, pleura, thymus and heart. World Health Organization Classification of Tumours. Lyon, France: IARC Press; 2004.
4. Brambilla E, Travis WD, Colby TV, Corrin B, Shimosato Y. The new World Health Organization classification of lung tumours. Eur Respir J. 2001;18(6):1059–68.
5. Gorshtein A, Gross DJ, Barak D, Strenov Y, Refaeli Y, Shimon I, et al. Diffuse idiopathic pulmonary neuroendocrine cell hyperplasia and the associated lung neuroendocrine tumors: clinical experience with a rare entity. Cancer. 2012;118(3):612–9.
6. Modlin IM, Bodei L, Kidd M. A historical appreciation of bronchopulmonary neuroendocrine neoplasia: resolution of a carcinoid conundrum. Thorac Surg Clin. 2014;24(3):235–55.
7. Davies SJ, Gosney JR, Hansell DM, Wells AU, du Bois RM, Burke MM, et al. Diffuse idiopathic pulmonary neuroendocrine cell hyperplasia: an under-recognised spectrum of disease. Thorax. 2007;62(3):248–52.
8. Lu YY, Chen JH, Liang JA, Chu S, Lin WY, Kao CH. 18 F-FDG PET or PET/CT for detecting extensive disease in small-cell lung cancer: a systematic review and meta-analysis. Nucl Med Commun. 2014;35(7):697–703.
9. Krenning EP, Kwekkeboom DJ, Bakker WH, Breeman WA, Kooij PP, Oei HY, et al. Somatostatin receptor scintigraphy with [111In-DTPA-D-Phe1]- and [123I-Tyr3]-octreotide: the Rotterdam experience with more than 1000 patients. Eur J Nucl Med. 1993;20(8):716–31.
10. Bini A, Grazia M, Stella F, Petrella F, Sellitri F, Fanti S, et al. The role of somatostatin receptor scintigraphy (Octreoscan) during follow-up of patients after bronchial carcinoid resection. A prospective study. J Cardiovasc Surg (Torino). 2005;46(3):318–9.
11. Zhernosekov KP, Filosofov DV, Baum RP, Aschoff P, Bihl H, Razbash AA, et al. Processing of generator-produced 68Ga for medical application. J Nucl Med. 2007;48(10):1741–8.
12. Virgolini I, Ambrosini V, Bomanji JB, Baum RP, Fanti S, Gabriel M, et al. Procedure guidelines for PET/CT tumour imaging with 68Ga-DOTA-conjugated peptides: 68Ga-DOTA-TOC, 68Ga-DOTA-NOC, 68Ga-DOTA-TATE. Eur J Nucl Med Mol Imaging. 2010;37(10):2004–10.
13. Surti S, Kuhn A, Werner ME, Perkins AE, Kolthammer J, Karp JS. Performance of Philips Gemini TF PET/CT scanner with special consideration for its time-of-flight imaging capabilities. J Nucl Med. 2007;48(3):471–80. 48/3/471.
14. Rindi G, Klersy C, Inzani F, Fellegara G, Ampollini L, Ardizzoni A, et al. Grading the neuroendocrine tumors of the lung: an evidence-based proposal. Endocr Relat Cancer. 2014;21(1):1–16.
15. Yokota J. Tumor progression and metastasis. Carcinogenesis. 2000;21(3):497–503.
16. Kuehl H, Veit P, Rosenbaum SJ, Bockisch A, Antoch G. Can PET/CT replace separate diagnostic CT for cancer imaging? Optimizing CT protocols for imaging cancers of the chest and abdomen. J Nucl Med. 2007;48 Suppl 1:45S–57S.
17. Fink G, Krelbaum T, Yellin A, Bendayan D, Saute M, Glazer M, et al. Pulmonary carcinoid: presentation, diagnosis, and outcome in 142 cases in Israel and review of 640 cases from the literature. Chest. 2001;119(6):1647–51.
18. Scott WJ. Surgical treatment of other bronchial tumors. Chest Surg Clin N Am. 2003;13(1):111–28.
19. Kayani I, Conry BG, Groves AM, Win T, Dickson J, Caplin M, et al. A comparison of 68Ga-DOTATATE and 18F-FDG PET/CT in pulmonary neuroendocrine tumors. J Nucl Med. 2009;50(12):1927–32.
20. Pavel M, Baudin E, Couvelard A, Krenning E, Oberg K, Steinmuller T, et al. ENETS Consensus Guidelines for the management of patients with liver and other distant metastases from neuroendocrine neoplasms of foregut, midgut, hindgut, and unknown primary. Neuroendocrinology. 2012;95(2):157–76.
21. Ferolla P, Daddi N, Urbani M, Semeraro A, Ribacchi R, Giovenali P, et al. Tumorlets, multicentric carcinoids, lymph-nodal metastases, and long-term behavior in bronchial carcinoids. J Thorac Oncol. 2009;4(3):383–7.
22. Schreiter NF, Nogami M, Steffen I, Pape UF, Hamm B, Brenner W, et al. Evaluation of the potential of PET-MRI fusion for detection of liver metastases in patients with neuroendocrine tumours. Eur Radiol. 2012;22(2):458–67.
23. Venkitaraman B, Karunanithi S, Kumar A, Khilnani GC, Kumar R. Role of (68)Ga-DOTATOC PET/CT in initial evaluation of patients with suspected bronchopulmonary carcinoid. Eur J Nucl Med Mol Imaging. 2014;41(5):856–64.
24. Jindal T, Kumar A, Venkitaraman B, Meena M, Kumar R, Malhotra A, et al. Evaluation of the role of [18F]FDG-PET/CT and [68Ga]DOTATOC-PET/CT in differentiating typical and atypical pulmonary carcinoids. Cancer Imaging. 2011;11:70–5.
25. Poeppel TD, Binse I, Petersenn S, Lahner H, Schott M, Antoch G, et al. 68Ga-DOTATOC versus 68Ga-DOTATATE PET/CT in functional imaging of neuroendocrine tumors. J Nucl Med. 2011;52(12):1864–70.
26. Prasad V, Baum RP. Biodistribution of the Ga-68 labeled somatostatin analogue DOTA-NOC in patients with neuroendocrine tumors: characterization of uptake in normal organs and tumor lesions. Q J Nucl Med Mol Imaging. 2010;54(1):61–7.
27. Travis WD, Giroux DJ, Chansky K, Crowley J, Asamura H, Brambilla E, et al. The IASLC Lung Cancer Staging Project: proposals for the inclusion of broncho-pulmonary carcinoid tumors in the forthcoming (seventh) edition of the TNM Classification for Lung Cancer. J Thorac Oncol. 2008;3(11):1213–23.

Lebenslauf

Mein Lebenslauf wird aus datenschutzrechtlichen Gründen in der elektronischen Version meiner Arbeit nicht veröffentlicht

Lebenslauf

Mein Lebenslauf wird aus datenschutzrechtlichen Gründen in der elektronischen Version meiner Arbeit nicht veröffentlicht

Lebenslauf

Mein Lebenslauf wird aus datenschutzrechtlichen Gründen in der elektronischen Version meiner Arbeit nicht veröffentlicht

Lebenslauf

Mein Lebenslauf wird aus datenschutzrechtlichen Gründen in der elektronischen Version meiner Arbeit nicht veröffentlicht

Lebenslauf

Mein Lebenslauf wird aus datenschutzrechtlichen Gründen in der elektronischen Version meiner Arbeit nicht veröffentlicht

Lebenslauf

Mein Lebenslauf wird aus datenschutzrechtlichen Gründen in der elektronischen Version meiner Arbeit nicht veröffentlicht

Lebenslauf

Mein Lebenslauf wird aus datenschutzrechtlichen Gründen in der elektronischen Version meiner Arbeit nicht veröffentlicht

Publication List

1: **Prasad V,** Steffen IG, Pavel M, Denecke T, Tischer E, Apostolopoulou K, Pascher A, Arsenic R, Brenner W. Somatostatin receptor PET/CT in restaging of typical and atypical lung carcinoids. EJNMMI Res. 2015 Dec;5(1):53. doi:10.1186/s13550-015-0130-2. Epub 2015 Oct 12. PubMed PMID: 26458908.

2: Pumberger M, **Prasad V**, Druschel C, Disch AC, Brenner W, Schaser KD. Quantitative in vivo fusion assessment by (18)F-fluoride PET/CT following en bloc spondylectomy. Eur Spine J. 2015 Sep 15. [Epub ahead of print] PubMed PMID: 26374129.

3: Bodei L, Kidd M**, Prasad V**, Modlin IM. Peptide Receptor Radionuclide Therapy of Neuroendocrine Tumors. Front Horm Res. 2015;44:198-215. doi: 10.1159/000402936. Epub 2015 Aug 14. PubMed PMID: 26303714.

4: Dilz LM, Denecke T, Steffen IG, **Prasad V**, von Weikersthal LF, Pape UF, Wiedenmann B, Pavel M. Streptozocin/5-fluorouracil chemotherapy is associated with durable response in patients with advanced pancreatic neuroendocrine tumours. Eur J Cancer. 2015 Jul;51(10):1253-62. doi: 10.1016/j.ejca.2015.04.005. Epub 2015 Apr 29. PubMed PMID: 25935542.

5: Kaemmerer D, Wirtz RM, Fischer EK, Hommann M, Sänger J, **Prasad V**, Specht E, Baum RP, Schulz S, Lupp A. Analysis of somatostatin receptor 2A immunohistochemistry, RT-qPCR, and in vivo PET/CT data in patients with pancreatic neuroendocrine neoplasm. Pancreas. 2015 May;44(4):648-54. doi: 10.1097/MPA.0000000000000316. PubMed PMID: 25872131.

6: Baur AD, Pavel M, **Prasad V**, Denecke T. Diagnostic imaging of pancreatic neuroendocrine neoplasms (pNEN): tumor detection, staging, prognosis, and response to treatment. Acta Radiol. 2015 Apr 8. pii: 0284185115579932. [Epub ahead of print] Review. PubMed PMID: 25855665.

7: Badakhshi H, Graf R, **Prasad V**, Budach V. The impact of 18 F-FET PET-CT on target definition in image-guided stereotactic radiotherapy in patients with skull base lesions. Cancer Imaging. 2014 Jun 25;14:25. doi: 10.1186/1470-7330-14-25. PubMed PMID: 25608761; PubMed Central PMCID: PMC4331830.

8: Kaul D, Badakhshi H, Gevaert T, Pasemann D, Budach V, Tuleasca C, Gruen A, **Prasad V**, Levivier M, Kufeld M. Erratum to: dosimetric comparison of different treatment modalities for stereotactic radiosurgery of meningioma. Acta Neurochir (Wien). 2015 Apr;157(4):565. doi: 10.1007/s00701-014-2315-2. PubMed PMID: 25530173.

9: Geisel D, Lüdemann L, Fröling V, Malinowski M, Stockmann M, Baron A, Gebauer B, Seehofer D, **Prasad V**, Denecke T. Imaging-based evaluation of liver function: comparison of ^{99}mTc-mebrofenin hepatobiliary scintigraphy and Gd-EOB-DTPA-

enhanced MRI. Eur Radiol. 2015 May;25(5):1384-91. doi: 10.1007/s00330-014-3536-8. Epub 2014 Dec 2. PubMed PMID: 25447973.

10: Kaul D, Badakhshi H, Gevaert T, Pasemann D, Budach V, Tuleasca C, Gruen A, **Prasad V**, Levivier M, Kufeld M. Dosimetric comparison of different treatment modalities for stereotactic radiosurgery of meningioma. Acta Neurochir (Wien). 2015 Apr;157(4):559-63; discussion 563-4. doi: 10.1007/s00701-014-2272-9. Epub 2014 Nov 21. Erratum in: Acta Neurochir (Wien). 2015 Apr;157(4):565. PubMed PMID:

25413163.

11: Bodei L, Sundin A, Kidd M, **Prasad V**, Modlin IM. The status of neuroendocrine tumor imaging: from darkness to light? Neuroendocrinology. 2015;101(1):1-17. doi: 10.1159/000367850. Epub 2014 Sep 10. PubMed PMID: 25228173.

12: Daniel K, Maria A, Amelie L, Isabell L, Stefan S, Luisa P, Merten H, **Prasad V**, Gerd B, Paul BR. Somatostatin receptor immunohistochemistry in neuroendocrine tumors: comparison between manual and automated evaluation. Int J Clin Exp Pathol. 2014 Jul 15;7(8):4971-80. eCollection 2014. PubMed PMID: 25197368; PubMed Central PMCID: PMC4152058.

13: Bodei L, Kidd M, **Prasad V**, Baum RP, Drozdov I, Modlin IM. The future of nuclear medicine imaging of neuroendocrine tumors: on a clear day one might see forever..... Eur J Nucl Med Mol Imaging. 2014 Dec;41(12):2189-93. doi: 10.1007/s00259-014-2836-1. PubMed PMID: 25047018.

14: Geisel D, Lüdemann L, Gebauer B, Fröling V, **Prasad V**, Heimann U, Stockmann M, Malinowski M, Hamm B, Brenner W, Denecke T. Optimized separation of left and right liver lobe in dynamic (99m)Tc-mebrofenin hepatobiliary scintigraphy using a hybrid SPECT-CT scanner. Ann Nucl Med. 2014 Nov;28(9):897-902. doi: 10.1007/s12149-014-0883-0. Epub 2014 Jul 10. PubMed PMID: 25008293.

15: **Prasad V,** Bodei L, Kidd M, Modlin IM. Whither peptide receptor radionuclide therapy for neuroendocrine tumors: an Einsteinian view of the facts and myths. Eur J Nucl Med Mol Imaging. 2014 Oct;41(10):1825-30. doi: 10.1007/s00259-014-2780-0. PubMed PMID: 24806111.

16: **Prasad V,** Brenner W, Modlin IM. How smart is peptide receptor radionuclide therapy of neuroendocrine tumors especially in the salvage setting? The clinician's perspective. Eur J Nucl Med Mol Imaging. 2014 Feb;41(2):202-4. doi: 10.1007/s00259-013-2593-6. PubMed PMID: 24196915.

17: Feyen O, Coy JF, **Prasad V,** Schierl R, Saenger J, Baum RP. EDIM-TKTL1 blood test: a noninvasive method to detect upregulated glucose metabolism in patients with malignancies. Future Oncol. 2012 Oct;8(10):1349-59. doi: 10.2217/fon.12.98. PubMed PMID: 23130932.

18: Kulkarni HR, **Prasad V**, Schuchardt C, Baum RP. Is there a correlation between peptide receptor radionuclide therapy-associated hematological toxicity and spleen dose? Recent Results Cancer Res. 2013;194:561-6. doi: 10.1007/978-3-642-27994-2_33. PubMed PMID: 22918783.

19: Schuchardt C, Kulkarni HR, **Prasad V**, Zachert C, Müller D, Baum RP. The Bad Berka dose protocol: comparative results of dosimetry in peptide receptor radionuclide therapy using (177)Lu-DOTATATE, (177)Lu-DOTANOC, and (177)Lu-DOTATOC. Recent Results Cancer Res. 2013;194:519-36. doi: 10.1007/978-3-642-27994-2_30. PubMed PMID: 22918780.

20: Todorović-Tirnanić M, Kaemmerer D, **Prasad V**, Hommann M, Baum RP. Intraoperative somatostatin receptor detection after peptide receptor radionuclide therapy with (177)Lu- and (90)Y-DOTATOC (tandem PRRNT) in a patient with a metastatic neuroendocrine tumor. Recent Results Cancer Res. 2013;194:487-96. doi: 10.1007/978-3-642-27994-2_28. PubMed PMID: 22918778.

21: Kulkarni HR, **Prasad V**, Kaemmerer D, Hommann M, Baum RP. High uptake of (68)Ga-DOTATOC in spleen as compared to splenosis: measurement by PET/CT. Recent Results Cancer Res. 2013;194:373-8. doi: 10.1007/978-3-642-27994-2_19. PubMed PMID: 22918769.

22: Kaemmerer D, Peter L, Lupp A, Schulz S, Sänger J, Baum RP, **Prasad V**, Hommann M. Comparing of IRS and Her2 as immunohistochemical scoring schemes in gastroenteropancreatic neuroendocrine tumors. Int J Clin Exp Pathol. 2012;5(3):187-94. Epub 2012 Mar 25. PubMed PMID: 22558472; PubMed Central PMCID: PMC3341681.

23: Swiętaszczyk C, **Prasad V**, Baum RP. Intense 18F-fluoride accumulation in liver metastases from a neuroendocrine tumor after peptide receptor radionuclide therapy. Clin Nucl Med. 2012 Apr;37(4):e82-3. doi: 10.1097/RLU.0b013e3182478a50. PubMed PMID: 22391729.

24: Salavati A, **Prasad V**, Schneider CP, Herbst R, Baum RP. Peptide receptor radionuclide therapy of Merkel cell carcinoma using (177)lutetium-labeled somatostatin analogs in combination with radiosensitizing chemotherapy: a potential novel treatment based on molecular pathology. Ann Nucl Med. 2012 May;26(4):365-9. doi: 10.1007/s12149-012-0578-3. Epub 2012 Feb 25. PubMed PMID: 22361935.

25: Kaemmerer D, **Prasad V,** Daffner W, Haugvik SP, Senftleben S, Baum RP, Hommann M. Radioguided surgery in neuroendocrine tumors using Ga-68-labeled somatostatin analogs: a pilot study. Clin Nucl Med. 2012 Feb;37(2):142-7. doi: 10.1097/RLU.0b013e3182291de8. PubMed PMID: 22228336.

26: Sainz-Esteban A, **Prasad V,** Schuchardt C, Zachert C, Carril JM, Baum RP. Comparison of sequential planar 177Lu-DOTA-TATE dosimetry scans with 68Ga-DOTA-TATE PET/CT images in patients with metastasized neuroendocrine tumours undergoing peptide receptor radionuclide therapy. Eur J Nucl Med Mol Imaging. 2012

Mar;39(3):501-11. doi: 10.1007/s00259-011-2003-x. Epub 2011 Dec 20. PubMed PMID: 22183108.

27: Oh S, **Prasad V**, Lee DS, Baum RP. Effect of Peptide Receptor Radionuclide Therapy on Somatostatin Receptor Status and Glucose Metabolism in Neuroendocrine Tumors: Intraindividual Comparison of Ga-68 DOTANOC PET/CT and F-18 FDG PET/CT. Int J Mol Imaging. 2011;2011:524130. doi: 10.1155/2011/524130. Epub 2011 Nov 9. PubMed PMID: 22121482; PubMed Central PMCID: PMC3216394.

28: Schreiter NF, Brenner W, Nogami M, Buchert R, Huppertz A, Pape UF, **Prasad V**, Hamm B, Maurer MH. Cost comparison of 111In-DTPA-octreotide scintigraphy and 68Ga-DOTATOC PET/CT for staging enteropancreatic neuroendocrine tumours. Eur J Nucl Med Mol Imaging. 2012 Jan;39(1):72-82. doi: 10.1007/s00259-011-1935-5. Epub 2011 Sep 17. PubMed PMID: 21927931.

29: Kaemmerer D, Peter L, Lupp A, Schulz S, Sänger J, **Prasad V,** Kulkarni H, Haugvik SP, Hommann M, Baum RP. Molecular imaging with ^{68}Ga-SSTR PET/CT and correlation to immunohistochemistry of somatostatin receptors in neuroendocrine tumours. Eur J Nucl Med Mol Imaging. 2011 Sep;38(9):1659-68. doi: 10.1007/s00259-011-1846-5. Epub 2011 May 31. PubMed PMID: 21626438.

30: Hommann M, Kaemmerer D, Daffner W, **Prasad V**, Baum RP, Petrovitch A, Sauerbrey A, Katenkamp K, Kaufmann R, Settmacher U. Nested stromal epithelial tumor of the liver--liver transplantation and follow-up. J Gastrointest Cancer. 2011 Dec;42(4):292-5. doi: 10.1007/s12029-010-9248-7. PubMed PMID: 21221846.

31: Shields CJ, Tiret E, Winter DC; International Rectal Carcinoid Study Group. Carcinoid tumors of the rectum: a multi-institutional international collaboration. Ann Surg. 2010 Nov;252(5):750-5. doi: 10.1097/SLA.0b013e3181fb8df6. PubMed PMID: 21037430.

32: Baum RP, **Prasad V**, Müller D, Schuchardt C, Orlova A, Wennborg A, Tolmachev V, Feldwisch J. Molecular imaging of HER2-expressing malignant tumors in breast cancer patients using synthetic 111In- or 68Ga-labeled affibody molecules. J Nucl Med. 2010 Jun;51(6):892-7. doi: 10.2967/jnumed.109.073239. Epub 2010 May 19. PubMed PMID: 20484419.

33: Fellner M, Baum RP, Kubícek V, Hermann P, Lukes I, **Prasad V**, Rösch F. PET/CT imaging of osteoblastic bone metastases with (68)Ga-bisphosphonates: first human study. Eur J Nucl Med Mol Imaging. 2010 Apr;37(4):834. doi: 10.1007/s00259-009-1355-y. Epub 2010 Jan 13. PubMed PMID: 20069291.

34: Sainz-Esteban A, **Prasad V**, Baum RP. Interesting image. Pancreatic neuroendocrine tumor with involvement of the inferior mesenteric vein diagnosed by Ga-68 DOTA-TATE PET/CT. Clin Nucl Med. 2010 Jan;35(1):40-1. doi: 10.1097/RLU.0b013e3181c3b74a. PubMed PMID: 20026975.

35: Kaemmerer D, **Prasad V**, Daffner W, Hörsch D, Klöppel G, Hommann M, Baum RP. Neoadjuvant peptide receptor radionuclide therapy for an inoperable neuroendocrine pancreatic tumor. World J Gastroenterol. 2009 Dec 14;15(46):5867-70. PubMed PMID: 19998512; PubMed Central PMCID: PMC2791284.

36: Baum RP, Swietaszczyk C, **Prasad V**. FDG-PET/CT in lung cancer: an update. Front Radiat Ther Oncol. 2010;42:15-45. doi: 10.1159/000262458. Epub 2009 Nov 24. Review. PubMed PMID: 19955789.

37: <u>Prasad V,</u> Ambrosini V, Hommann M, Hoersch D, Fanti S, Baum RP. Detection of unknown primary neuroendocrine tumours (CUP-NET) using (68)Ga-DOTA-NOC receptor PET/CT. Eur J Nucl Med Mol Imaging. 2010 Jan;37(1):67-77. doi: 10.1007/s00259-009-1205-y. Epub . PubMed PMID: 19618183.

38: Singh B, Sunil HV, Sharma S, **Prasad V**, Kashyap R, Bhattacharya A, Mittal BR, Taneja A, Rai R, Goni VG, Aggarwal S, Gill SS, Bhatnagar A, Singh AK. Efficacy of indigenously developed single vial kit preparation of 99mTc-ciprofloxacin in the detection of bacterial infection: an Indian experience. Nucl Med Commun. 2008 Dec;29(12):1123-9. doi: 10.1097/MNM.0b013e328318b369. PubMed PMID: 18987535.

39: Tuli HS, Singh B, **Prasad V**, Das A, Gupta AK, Mittal BR. Diagnostic accuracy of 99mTc-MIBI-SPECT in the detection of lymph node metastases in patients with carcinoma of the tongue: comparison with computed tomography and MRI. Nucl Med Commun. 2008 Sep;29(9):803-8. doi: 10.1097/MNM.0b013e328302ccfa. PubMed PMID: 18677208.

40: Singh B, **Prasad V**, Bhattacharya A, Singh AK, Bhatnagar A, Mittal BR, Gupta KA. Diagnosis of mandibular osteomyelitis in probable coexisting tumor recurrence: role of Tc-99m ciprofloxacin imaging. Clin Nucl Med. 2008 Aug;33(8):525-7. doi: 10.1097/RLU.0b013e31817e6de9. PubMed PMID: 18645368.

41: <u>Prasad V</u>, Fetscher S, Baum RP. Changing role of somatostatin receptor targeted drugs in NET: Nuclear Medicine's view. J Pharm Pharm Sci. 2007;10(2):321s-337s. Review. PubMed PMID: 17718935.

42: Singh B, Manoj R, **Vikas P**, Bhattacharya A, Sharma Y, Mittal BR. Comparison of left ventricular functional parameters measured by gated single photon emission tomography and by two-dimensional echocardiography. Hell J Nucl Med. 2006 May-Aug;9(2):94-8. PubMed PMID: 16894412.

43: Rai Mittal B, Singh S, Bhattacharya A, **Prasad V**, Singh B. Lung scintigraphy in the diagnosis and follow-up of pulmonary thromboembolism in children with nephrotic syndrome. Clin Imaging. 2005 Sep-Oct;29(5):313-6. PubMed PMID: 16153536.

44: Bhattacharya A, **Prasad V**, Thomas EJ, Singh B, Mittal BR. Ectopic kidneys as a source of misinterpretation on bone scintigraphy. Clin Nucl Med. 2005 Jul;30(7):503-5. PubMed PMID: 15965331.

45: Bhattacharya A, **Prasad V**, Thomas EJ, Singh B, Mittal BR. Tc-99m MDP scintigraphy in a case of idiopathic calcinosis cutis. Clin Nucl Med. 2005 Jun;30(6):431-2. PubMed PMID: 15891303.

46: Bhattacharya A, **Prasad V**, Mittal BR. Tc-99m MDP uptake in a soft tissue hematoma of the chest wall. Clin Nucl Med. 2004 Jul;29(7):454-5. PubMed PMID: 15192477.

47: Lanka KP, Sarin B, **Prasad V**, Sen S, Mehta A, Rawat HS, Mondal A, Sharma R. Benign cervical thymoma masquerading as a malignant thyroid nodule. Clin Nucl Med. 2002 Dec;27(12):862-4. PubMed PMID: 12607863.

48: Bodei L, Kidd M, Modlin IM, **Prasad V**, Severi S, Ambrosini V, Kwekkeboom DJ, Krenning EP, Baum RP, Paganelli G, Drozdov I. Gene transcript analysis blood values correlate with ^{68}Ga-DOTA-somatostatin analog (SSA) PET/CT imaging in neuroendocrine tumors and can define disease status. Eur J Nucl Med Mol Imaging. 2015 Aug;42(9):1341-52. doi: 10.1007/s00259-015-3075-9. Epub 2015 May 7. PubMed PMID: 25947577.

49: <u>**Prasad V,**</u> Baum RP. Biodistribution of the Ga-68 labeled somatostatin analogue DOTA-NOC in patients with neuroendocrine tumors: characterization of uptake in normal organs and tumor lesions. Q J Nucl Med Mol Imaging. 2010 Feb;54(1):61-7. PubMed PMID: 20168287.

50. Knie B, Plotkin M, Zschieschang P, Prasad V, Moskopp D. A family with pheochromocytoma-paraganglioma inherited tumour syndrome. Serial 18F-DOPA PET/CT investigations. Nuklearmedizin. 2016 Jan 7;55(1). [Epub ahead of print]

Book Chapters

1. Richard. P. Baum, **Vikas Prasad**: Molecular Imaging:- Treatment Monitoring: 4th Edition of Clinical Nuclear Medicine Eds: Maisey, Britton, Cook, Chenagzi. Hodder Arnold Publishers, 2007

2. Richard P Baum, **Vikas Prasad**, Wolfgang Weber :Lung Cancer. In: Advances in Nuclear Oncology - Diagnosis and Therapy, Emilio Bombardieri John Buscombe, Giovanni Lucignani, Otmar Schober Eds, Francis and Taylor

3. Richard P Baum, **Vikas Prasad**, Juan P. Oliva González. Radioimmunotherapy. In: Nuclear Medicine Concise, Biersack, Freeman (eds), Springer-Verlag. Chap 26; 467-490

4. Richard P Baum, Vikas Prasad. PET Imaging of Neuroendocrine Tumors. In: Principles and Practice of Positron Emission Tomography. Richard Wahl, Julia W. Buchanan. Lippincott Williams and Wilkins

5. Richard P Baum, **Vikas Prasad**, Maria Lucia Calcagni. Diagnóstico de los tumores cerebrales con aminoácidos radiactivos in Neuromedicina Nuclear. Eds José Manuel Castro Beiras, Juan Perfecto Oliva González, Patricia Paredes Rodríguez, Juan José Martínez Sampere, Joaquín González González, Maipa Orduña, José Antonio Arias Navalón

6. Vikas Prasad, V. Ambrosini, S. Fanti, R. P. Baum. PET/CT in neuroendocrine tumors: evaluation of receptors status and metabolism. In PET Clinic (2008) Publisher: Elseiver, Eds: Abbas Alavi, S. Fanti

7. Vikas Prasad, Nils Schreiter, Winfried Brenner. Nuklearmedizinische Verfahren bei neuroendokrinen Tumoren des Magen-Darm-Traktes. Endokrine Chirurgie (2011)

8. Vikas Prasad, Winfried Brenner. Nuklearmedizinische Therapie bei metastasierten neuroendokrinen Tumoren. Endokrine Chirurgie (2011)

Acknowledgement